Effects of Interstitial Flow on Tumor Cell Migration

by

William J. Polacheck
B.S. Biological Engineering
Cornell University, 2008

SUBMITTED TO THE DEPARTMENT OF MECHANICAL ENGINEERING IN PARTIAL FUFILLMENT OF THE REQUIREMENTS FOR THE DEGREE OF

MASTER OF SCIENCE IN MECHANCIAL ENGINEERING
AT THE
MASSACHUSETTS INSTITUTE OF TECHNOLOGY

JUNE 2010

ARCHIVES

Signature of Author.....
Department of Mechanical Engineering
May 7, 2010

Certified by.....
Roger Kamm
Professor of Mechanical Engineering and Biological Engineering
Thesis Supervisor

Accepted by:.....
David Hardt
Professor of Mechanical Engineering
Chairman, Committee for Graduate Students

Effects of Interstitial Flow on Tumor Cell Migration

by

William J. Polacheck

Submitted to the Department of Mechanical Engineering on May 7th, 2010 in Partial Fulfillment of the Requirements for the Degree of Master of Science in Mechanical Engineering

Abstract

Interstitial flow is the convective transport of fluid through tissue extracellular matrix. This creeping fluid flow has been shown to affect the morphology and migration of cells such as fibroblasts, cancer cells, endothelial cells, and mesenchymal stem cells. However, due to limitations in experimental procedures and apparatuses, the mechanism by which cells detect flow and the details and dynamics of the cellular response remain largely unknown. We developed a microfluidic cell culture system in which we can apply stable pressure gradients and fluid flow, and in which we can observe transient responses of breast cancer cells seeded in a 3D collagen type I scaffold. We employed this system to examine cell migration in the presence of interstitial flow to address the hypothesis that interstitial flow increases the metastatic potential of breast cancer cells. By varying the concentration of chemoattractants, we decoupled the mechanisms that provide the migratory stimulus and the directional stimulus to migrating breast cancer cells in the presence of a flow field. We found that cells migrated along streamlines in the presence of flow and that the strength of the flow field determined directional bias of migration along the streamline. We provide evidence that CCR7-dependent autologous chemotaxis is the mechanism by which cells migrate with the flow, while a competing CCR7-independent mechanism leads to migration against the flow. Furthermore, we demonstrate these competing mechanisms are a powerful migrational stimulus, which likely play an important role in development of metastatic disease.

Thesis supervisor: Roger Kamm
Title: Professor of Mechanical and Biological Engineering

Acknowledgements

I would like to thank my advisor, Roger Kamm, for his patience and invaluable advice on topics ranging from experimental techniques to outlook on education and science. He has instilled confidence and understanding that engineering, through its tenets of design and quantitative rigor, can provide powerful insight into biological science.

I also thank The Charles Stark Draper Laboratory for financial support, and in particular, Drs. Joe Charest and Jeff Borenstein for a much needed industry perspective on our devices and experiments.

I would also like to thank the graduate students and post-docs who have helped out along the way. Yannis Zervantonakis for training me and engaging me in countless conversations, both supportive and critical, about microfluidics, cell culture, and experiment design. Nate Hammond for his Matlab expertise and entertaining conversations that provide a refreshing break from lab work. Drs. Seok Chung and Ryo Sudo provided valuable guidance on device design and cell culture. Cherry Wan and Joy Rimchala not only helped optimize my cell culture technique but also frequently saved my cells from a variety of perils.

My family has supported me every step of the way, and I cannot thank them enough for that. In constantly striving for intellectual stimulation, my family has taught me there is always something new to be learned. My parents are true role models, and their ability to maintain professional excellence while raising a family is an inspiration. The countless conversations with my sister about the arts, architecture, and religion repeatedly remind me that mathematics isn't everything and that engineers aren't better than everyone else.

This work is supported by a National Science Foundation Graduate Research Fellowship.

Table of Contents

Abstract 3

1. Introduction 11
- 1.1. Tissue interstitium 11
- 1.2. Metastasis and tumor cell migration 12
- 1.3. *In vitro* systems for investigating cell behavior 13
- 1.4. Chemotaxis 13
- 1.5. Epidermal growth factor 14
- 1.6. CCR7 and CCL21 15
- 1.7. Autologous chemotaxis 15

2. Objective 19

3. Materials and Methods 21
- 3.1. Device Design Requirements 21
- 3.2. System Design. 21
- 3.3. Cell and Device Preparation. 23
- 3.4. Establishing interstitial flow. 24
- 3.5. Imaging and image processing 25

4. Results 27
- 4.1. System design and geometry 27
- 4.2. Interstitial flow field verification 28
- 4.3. 3D cell culture 32
- 4.4. Cell alignment 34
- 4.5. Cell morphology 36
- 4.6. Cell migration. 37
- 4.7. Migration along streamlines. 39
- 4.8. Directional bias along streamlines. 41
- 4.9. Effect of EGF on migration direction 43
- 4.10. Effect of cell density. 44
- 4.11. Effect of blocking CCR7 signaling pathway. 47
- 4.12. Effect of blocking CCR7 signaling pathway and reducing cell density. 50
- 4.13. Summary of directional bias in migration 55

5. Discussion 57
- 5.1. Microfluidic platform 57
- 5.2. Cell alignment 57
- 5.3. Effect of interstitial flow on cell migration 58
- 5.4. Effects of interstitial flow on direction of cell migration 59
- 5.5. Cellular transport environment with interstitial flow 60
- 5.6. Autologous chemotaxis 61
- 5.7. Competing signals 63
- 5.8. Shear stress and mechanotransduction 67
- 5.9. Other possible competing pathways 68

6. Conclusion 71

Appendix I – Migration bias expressed as fractions of migrating cells 73

Appendix II – Total streamline and directional migration scores 75

References: 80

Index of Figures, Equations, and Tables.

Figure 1: Transcellular autocrine gradients for a cell exposed to interstitial flow. Color bar represents low to high concentration. The Pe is 0.7 (adapted from 6)..... 17

Figure 2: Modified Boyden chamber used by Shields et al. Cells are seeded on an insert and the number of cells that migrate through the membrane are quantified (adapted from 6). 18

Figure 3: Set-up for applying interstitial flow 22

Figure 4: Microfluidic system for seeding cells and applying interstitial flow. Cells are seeded in the central region, and the media channels are connected to external reservoirs to apply a hydrostatic pressure gradient. P1 ad P0 are pressures in the two channels with P1>P0 to generate flow through the gel. 28

Figure 5: FEM solution of Brinkman's equation in the region of interest for the microfluidic system. 29

Figure 6: Superimposed fluorescent image of microspheres and phase contrast image of the region of interest in the device. Green vectors indicate magnitude and direction of tracked beads, and blue vectors indicate local predicted magnitude and direction of the flow field from the FEM model..... 29

Figure 7: Magnitude of observed velocity and magnitude of velocity predicted by Brinkman's equation. Nominal values are labeled on the x-axis. 31

Figure 8: Average local deviation between the measured angle of the velocity vector and that predicted by the FEM. Dashed line indicates average value for a random distribution of angles. 31

Figure 9: Confocal z-stack (labels indicate height from coverslip) of GFP expressing MDA-MB-231 cells in collagen I gel. 32

Figure 10: Time lapse images (every 60min) of a cell migrating in 3D in collagen gel. 33

Figure 11: Superimposed confocal reflectance image of cells seeded in 3D collagen I matrix (blue) and confocal image of GFP expressing MDA-MB-231 cells (green). Gap behind cell (red arrow) shows cells migrate in 3D, degrading matrix during migration. 33

Figure 12: A) Phase contrast image of cells aligned to flow. Flow velocity vectors are overlaid in blue. B) DAPI and phalloidin stain after 36hrs in flow field. Cells form strings after longer times in culture. White arrow indicates direction of flow. 35

Figure 13: Percent of cell population aligned with flow streamlines. Threshold angle for alignment is 45 degrees..... 35

Figure 14: Effect of interstitial flow on cell morphology. Interstitial flow elongates cells, but there is a time delay to increased elongation. 36

Figure 15: Average migration velocity for cells exposed to flow. Migration velocity magnitude was independent of interstitial flow rate. 37

Figure 16: The effect of interstitial flow on average directionality, defined as net migration distance normalized by total migration distance. Cells exposed to flow showed increased directionality. 38

Figure 17: The effect of interstitial flow on cell motility, defined as the fraction of cell population migrating a distance of more than one cell diameter. Motility was not a function of low rate. 38

Figure 18: Schematic of scores used to quantify direction of cell migration. Blue arrow indicates streamline. (a) Streamline migration score is used to determine relative population of cells migrating along the streamline. (b) Directional migration score is used to determine bias of migration with or against flow. 40

Figure 19: Polar histogram of migration direction for (a) control and (b) cells exposed to 3.0μm/s flow. Flow induced directional bias in migrating cells. 40

Figure 20: Average streamline migration score for cells exposed to flow. Cells exposed to interstitial flow preferentially migrated along streamlines, although to a lesser extent at the higher flow rate. 41

Figure 21: Average directional migration score for cells exposed to flow. Cells at high flow rate show a significant bias for migration in the upstream direction. 42

Figure 22: Streamline and directional migration scores for devices at 10ng/ml EGF and a saturation concentration of 50ng/ml. Saturating the devices with EGF did not effect directional bias of cell migration indicating that directional bias is not due to EGF gradients. 43

Figure 23: Motility was not a function of intercellular distance 44

Figure 24: Directionality was not a function of intercellular distance 45

Figure 25: Increased intercellular distance caused a reduction in migration velocity, but the difference was not statistically significant. 45

Figure 26: Effect of reducing cell density on migration along streamline. At high interstitial flow rates, increasing intercellular distance decreased biased migration along streamlines. 46

Figure 27: Effect of reducing cell density on directional bias of migration. Increasing intercellular distance caused significant migrational bias in the direction of flow 47

Figure 28: Effect of blocking CCR7 signaling pathway on motility. Blocking CCR7 caused a significant decrease in motility for cells not exposed to flow, but interstitial flow recovered this decrease 48

Figure 29: Effect of blocking CCR7 pathway on migration velocity. Blocking CCR7 caused a significant decrease in migration velocity for cells not exposed to flow, but this decrease was recovered in cells exposed to flow..... 48

Figure 30: Effect of blocking CCR7 pathway on directionality of migrating cells. Blocking CCR7 caused a decrease in directionality of migration..... 49

Figure 31: Effect of blocking CCR7 signaling on migration along streamlines. At low flow rates, blocking CCR7 signaling caused a significant decrease in migration along streamlines..... 49

Figure 32: Effect of blocking CCR7 signaling on directional bias of migration along streamlines. Blocking CCR7 caused an increase in directional bias of migration against the flow..... 50

Figure 33: Effect of CCR7 blocking at low cell concentrations on motility of cell population... 51

Figure 34: Effect of blocking CCR7 on migration velocity at low cell concentrations 52

Figure 35: Effect of blocking CCR7 signaling on directionality of migration. Blocking CCR7 reduced directionality of migrating cells exposed to flow..... 52

Figure 36: Effect of blocking CCR7 signaling on directional migration of cells..... 53

Figure 37: Effect of blocking CCR7 signaling at low cell concentrations on directional bias of migration along streamlines. Blocking CCR7 causes a reversal in directional bias for migrating cells..... 53

Figure 38: Effect of intercellular distance on directional bias of migration for cells with blocked CCR7 pathways. Intercellular distance does not affect the migration profiles of cells when CCR7 is blocked. 54

Figure 39: Effect of intercellular distance on directional bias of cells migrating along streamlines. Intercellular distance does not affect directional bias for cells with blocked CCR7 pathways. 54

Figure 40: Effect of Peclet # on transcellular distribution of autocrine morphogens. Flow is from left to right. Plotted is normalized concentration, red is maximum and blue minimum concentration. Adapted from Fleury et al. (8)..... 61

Figure 41: Transport model for demonstrating the effect of cell density on transcellular autocrine chemokine gradients. Normalized concentration, with red maximum concentration and blue minimum concentration. All parameters are the same in both figures, except intercellular distance. 63

Figure 42: Average streamline migration score for each experimental condition. Error bars are omitted for clarity. Note peak at 0.3μm/s for cells with functional CCR7 receptors. 66

Figure 43: Average directional migration score for each experimental condition. Note that seeding density does not affect migration directional bias when CCR7 is blocked. 66

Figure 44: Model of pressure gradient on a cell surface induced by interstitial flow. Flow is from left to right, red indicates maximum force, blue indicates minimum force. High force on the surface of the cell can induce FA formation and directional migration (adapted from 51).. 68

Figure 45: Fraction of cell population migrating along streamline for each set of experimental conditions. 73

Figure 46: Of cells migrating along streamline, the fraction of cells migrating upstream. 74

Figure 47: Summary of streamline migration scores for cells at each experimental condition. (♦,✚ indicate significance for similarly labeled data sets) 78

Figure 48: Summary of directional migration scores for cells at each experimental condition. . 79

Equation 1: Darcy's Law 11

Equation 2: Peclet number 16

Equation 3: Brinkman's equation 25

Table 1: Summary of streamline and directional scores for cell populations (mean±SEM) 76

Table 2: Summary of comparisons between experimental conditions. P-values given from student's t-test 77

1. Introduction

1.1. Tissue interstitium

Tissues are comprised of cells residing in an extracellular matrix (ECM). The ECM is a tissue-specific network of molecules, typically consisting of collagens, proteoglycans, and laminins (1). The ECM provides mechanical support to cells and affects cell signaling through force transduction and cytokine binding (6,18). ECM composition, architecture, and mechanical properties have been shown to affect gene expression and cell function (17-20). Tissues and the ECM are bathed in fluid that carries nutrients and signaling molecules to cells in the tissue (44). Osmotic and hydrostatic pressure gradients across tissues resulting from physiologic processes such as lymphatic draining, inflammation, and muscle contraction drive fluid flow through the ECM (21). On a macroscopic scale, this fluid flow is modeled by Darcy's Law (Equation 1),

$$\underline{v} = -K\nabla P$$

Equation 1: Darcy's Law

Which relates fluid velocity to pressure drop across a porous material with permeability, K. The flow of fluid through tissue is termed interstitial flow and has long been postulated to play a critical role in tissue transport and physiology (2).

Chary and Jain used fluorescence recovery after photobleaching to directly observe fluid flow in the tissue interstitium and determined typical flow velocities to be on the order of 0.1-2.0μm/s, and more recent studies have demonstrated that flow can reach velocities up to 4.0μm/s (3,9). Interstitial flow is particularly important in driving transport in tumor tissues, as neoplastic tissue is often characterized by increased interstitial pressure (4). The high interstitial pressure is due to osmotic and hydrostatic pressure resulting from blood vessel leakiness, lymph vessel abnormalities, interstitial fibrosis, and contraction of the interstitial space (47). The increased

interstitial pressure in neoplastic tissues causes large pressure gradients and consequently large interstitial flow velocities, in the tumor margin where cancerous tissue meets non-neoplastic tissue (22).

1.2. Metastasis and tumor cell migration

Breast cancer incidence in the United States is approximately 1 in 8, and 40,480 women died from breast cancer in 2008 (24). Over 90% of breast cancer related deaths are due to metastases, secondary tumors at a site distant from the primary tumor (23). In the formation of metastases, tumor cells abandon the native epithelial phenotype and migrate from the primary tumor to vasculature as single cells or as a collective invasive front (40). Cells then enter the vasculature through a process known as intravasation, and subsequently the systemic circulation carries cells to a distant part of the body (52). Eventually cells extravasate through vasculature into tissue and form a secondary tumor at a site distant from the primary tumor (26). Although much recent work has focused on understanding the genetic and molecular expression of cancer and metastatic cells, little is known about the mechanics and dynamics that drive tumor cells leaving the primary tumor and migrating to vasculature or lymphatic vessels.

High intratumoral interstitial pressure has been correlated with highly metastatic tumors, and interstitial flow has emerged as a possible stimulus for guiding tumor cell migration in the formation of metastases (5, 31, 45, 53). In the metastatic process, breast cancer cells undergo a transformation known as the epithelial to mesenchymal transition (EMT), where they lose the characteristic phenotype of natural striated tissue and acquire a migratory phenotype (25). Consequently, recent work on interstitial flow and cancer has been focused on the response of single, migratory cancer cells to a convective flow field of physiological magnitude (5).

1.3. *In vitro* systems for investigating cell behavior

Understanding the details and dynamics of metastasis is complicated by the myriad of cell types, signaling molecules, ECM components, and cellular interactions involved in EMT, migration, and intravasation. Consequently, *in vitro* systems have been developed to isolate the effects of an individual stimulus on steps of the metastatic cycle (5-7,31,35-37,41,47). Typically these systems involve one or multiple cell types seeded on a surface or in a gel of reconstituted ECM components. Microfluidics has emerged as a powerful tool for manipulating molecular concentrations, molecular gradients, and physical stimuli to cells seeded in these systems. In particular, soft lithography allows for the construction of cellular bioreactors with small length scales and sample sizes, rapid prototyping, and optical properties that allow for live-cell imaging (35-37). Although *in vitro* systems have been developed to isolate effects of pressure gradients and flow on cell physiology, the physiological relevance of these systems is limited by 2D or pseudo-3D culture, where cells are seeded on a surface and overlaid with a gel (5-7). Furthermore, many systems are not designed to allow live-cell imaging to observe cell dynamics and cellular responses in real-time.

1.4. Chemotaxis

Cellular migration *in vivo* and *in vitro* is dependent on both the physical and biochemical properties of cells and ECM (54). Recent work has shown cells can sense the mechanical stiffness of their physical environment, and environmental stiffness can lead to changes in cellular gene expression and phenotype (55). Furthermore, *in vitro* experiments involving cells seeded in gels with encapsulated fluorescent microspheres have shown that cells preferentially migrate toward mechanically stiffer substrate, a phenomenon called durotaxis (56-58).

Much work has focused on the role of chemokines, a superfamily of cytokine-like proteins, in directing cell migration. These proteins are secreted by cells and interact with G-protein-coupled receptors to cause cytoskeletal rearrangement and induce directionally oriented migration (15-20). Chemokines can induce migration toward increasing concentration of a chemoattractant or migration toward a decreasing concentration of a chemorepellant. Chemokine signaling in which a cell responds to a self-secreted chemokine is known as autocrine signaling, as opposed to paracrine signaling in which a cell responds to a chemokine secreted by a neighboring cell (6). Both autocrine and paracrine signaling are well-established mechanisms that drive tumor cell phenotype and migration (25).

1.5. Epidermal growth factor

An important growth factor and chemokine with demonstrated significance in tumor cell migration, inflammation, and wound healing is epidermal growth factor (EGF). EGF and the associated cell-surface receptor, EGFR, have been studied in detail *in vivo* and *in vitro* to determine the role of EGF in tumor cell migration (32-37). The presence of EGFR is correlated with poor outcome in human breast cancer cases, and Price et al. showed that the correlation arises from strong cellular chemotactic response to EGF as opposed to previously hypothesized proliferative response. They also demonstrated that a far greater percentage of a cancer cell population migrates beyond one cell diameter in the presence of supplemental EGF as compared to standard culture medium (60). Saadi et al. employed a microfluidic system to demonstrate that speed of tumor cell migration is a function of the magnitude of EGF concentration and that directionality and direction of migration are affected by magnitude and direction of an EGF molecular gradient (34). Furthermore, it has been shown that cellular response to EGF gradients

is due to differential receptor binding across the length of a cell. Cells extend protrusions and migrate in the direction of highest receptor occupation (43).

1.6. CCR7 and CCL21

Recent *in vitro* studies have demonstrated tumor cell migration potential is well correlated with expression of two chemotactic receptors, CCR7 and CXCR4, and *in vivo* experiments have demonstrated that blocking these two receptors decreases the incidence of metastasis (28-32). CCR7 and CXCR4 binding induce actin polymerization and pseudopodia formation, resulting in increased cell motility (28). Quantitative reverse transcription polymerase chain reaction (RT-PCR) experiments have confirmed high expression levels of CCR7 and CXCR4 in commonly used invasive breast carcinoma cell lines, including MDA-MB-231 (30). Furthermore, organs that are frequent sites of metastasis formation demonstrate high levels of expression of the ligands to these receptors (29). CCR7 is of particular interest in understanding metastasis because CD4+ T cells and dendritic cells require CCR7 expression to migrate through lymphatic vessels (49). Because lymphatic vessels function as the sink for interstitial flow, it has been postulated that interstitial flow and CCL21, an anti-CCR7 ligand, act in conjunction to guide migrating tumor cells to lymphatics in the formation of metastases (5).

1.7. Autologous chemotaxis

Recent work has demonstrated that interstitial flow leads to CCR7 activation and can influence breast cancer cell migration even in the absence of lymphatic cells. Shields et al. developed a modified Boyden chamber assay to investigate the mechanism by which interstitial flow induces CCR7-dependent cell migration in breast cancer cell cultures. The authors observed increased metastatic potential in cell populations exposed to flow and demonstrated the increased

metastatic potential was activated through binding of self-secreted CCL21 ligand to the CCR7 receptor (5). This autocrine signaling mechanism, called autologous chemotaxis, arises in a flow field where convection distributes autocrine factors leading to a transcellular concentration gradient, which provides a chemotactic signal (10). The magnitude of the transcellular autocrine gradient is governed by molecular diffusion and convection of the chemokine the Peclet number represents the ratio of convective to diffusive transport (Equation 2),

$$\mathrm{Pe} = \frac{VL}{D}$$

Equation 2: Peclet number

where V is the magnitude of the fluid velocity, L is a characteristic length, and D is the molecular diffusivity of the given molecule in the given medium. For Pe<<1, transport is diffusion dominated, and autocrine gradients will be insignificant, and for Pe>>1, transport is convection dominated, and autocrine chemokines are washed downstream. There exists an intermediate region, for Pe ~ 1, where transport is neither diffusion dominated nor convection dominated. In this transport regime, diffusion transports the chemokine radially outward from the cell and convection transports chemokine downstream at a rate that allows for the chemokine to bind to cell surface receptors. Competing convection and diffusion causes the autocrine chemokine to be highly concentrated at the downstream surface of the cell, and less concentrated at the upstream surface of the cell, resulting in a transcellular gradient (Figure 1, 8).

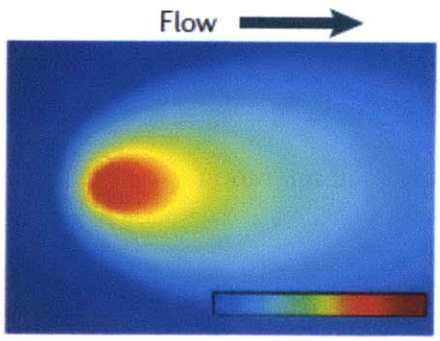

Figure 1: Transcellular autocrine gradients for a cell exposed to interstitial flow. Color bar represents low to high concentration. The Pe is 0.7 (adapted from 6).

Although computational modeling confirms Pe-dependent transcellular autocrine chemokine gradients, the simulations have been limited to modeling single cells suspended in homogenous ECM (8). Presumably the magnitude and profile of autocrine gradients are a function of cell density. At high cell density, autocrine chemokine fields interact with paracrine chemokine fields from neighboring cells. However, the effect of cell density on autocrine gradients has not been explored computationally or experimentally.

Development of the autologous chemotaxis model has been limited to experiments performed in a Boyden chamber, in which cells are seeded on a membrane, and migrating cells are quantified as the number of cells that migrate through the membrane. Consequently, only cells that migrate in one direction, downstream through the membrane, are quantified in this assay. It has yet to be determined whether the observed downstream migration with interstitial flow in the experiments of Shields *et al.* is due to directed cell migration in the direction of the flow, or if the migration response is more complicated but interpretation is impaired by the fact that only downstream migration is observed. The directional bias of migration is an important piece to validating the autologous chemotaxis model, as convectively distributed autocrine chemoattractant gradients

can bias migration in the downstream direction only. We developed a system where directional bias of migration can be observed, and we address the validity of the autologous chemotaxis model in the context of 3D directed cell migration.

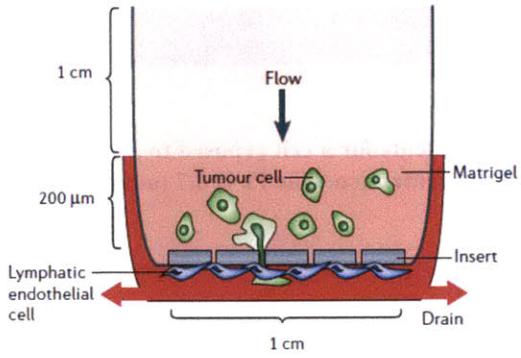

Figure 2: Modified Boyden chamber used by Shields et al. Cells are seeded on an insert and the number of cells that migrate through the membrane are quantified (adapted from 6).

2. Objective

The objective of this project encompasses design and scientific discovery. In order to investigate interstitial flow as a stimulus for tumor cell migration, we must first design a system that allows for the application of a repeatable and predictable interstitial flow field while sustaining high cell viability. Furthermore, to improve upon previously used culture systems, our system must provide robust, repeatable observation of live-cell dynamics for cells seeded in a physiologically relevant 3D matrix.

With this platform for culturing cells, we will investigate interstitial flow as a migration stimulus. We plan to investigate parameters that could not be observed with previous systems, such as migration velocity, directional characteristics of migration, and cell morphology and phenotype. In performing a complete investigation of the directional characteristics of cell migration in the presence of flow, we will also address the validity of the autologous chemotaxis model. We plan to address migration parameters as a function of cell density and chemokine receptor blocking. In so doing, we will examine the effects of interstitial flow on tumor cell migration and help elucidate the mechanisms by which cells sense and respond to interstitial flow.

3. Materials and Methods

3.1. Device Design Requirements.

In order to fulfill the objectives presented above, we need to design an experimental apparatus in which we can culture cells, subject cells to a repeatable and predictable flow field, and maintain high cell viability. To ensure experimental repeatability, the system must be easily fabricated and system variability must be low. The system needs to be optically transparent and biocompatible to allow imaging and to maintain high cell viability. The system must be easily transferred from the incubator to imaging stage and easily sterilized to avoid bacterial and fungal contamination.

In order to improve upon previous devices and provide greater physiological relevance, cells must be suspended in a 3D matrix of reconstituted ECM components. Consequently, the system must include a region where cell-matrix suspension can be added and polymerized. A pressure drop is needed to drive fluid flow through the 3D cell construct, so the system must be closed to the atmosphere but allow input and outlet ports for sterile cell media. The geometry of the flow chamber must be simple so the pressure drop induces a predictable flow field.

3.2. System Design.

Microfluidic devices have emerged as powerful instruments for cell culture and engineering the cellular microenvironment (6, 64, 65). In particular, soft lithography is an efficient, cheap, and robust technique for fabricating biocompatible microfluidic devices (7, 63). We have developed a microfluidic system that is fabricated using soft lithography and meets the design requirements mentioned above. The system consists of a microfluidic chip, fabricated from polydimethysiloxane (PDMS), with etched features including a cell culture region and media

ports. The PDMS chip can be autoclaved and is sealed with a glass coverslip to allow for sterile cell culture. Media channels are connected to the chip with polyethelyne tubing, and outlet valves allow aspiration of gas bubbles that may form in the media channels during thermal equilibration.

Figure 3 provides images and a schematic of the device. In Figure 3a, the whole setup is shown. The system was designed so that all components could fit on a petri dish for easy transportation to and from the incubator. The media reservoirs can be seen along with the tubing and valves to allow aspiration of gas bubbles. Figure 3b shows a close-up of the PDMS microfluidic device disconnected from the media reservoirs. These devices are easily fabricated; total fabrication, sterilization, and surface treatment time for each set of devices is less than 3 days, including all incubation periods, and the number of devices in a set is limited only by the size of a silicon wafer. Typically 4 devices are made at a time. Figure 3c is a schematic of the cell culture region within the device. The pink area in the middle of the schematic is the region where collagen-cell suspension is added and polymerized, and the blue and green regions are the media channels, which are connected to the external media reservoirs. Each white square post has a side length of 250μm. More details of the device design are discussed below.

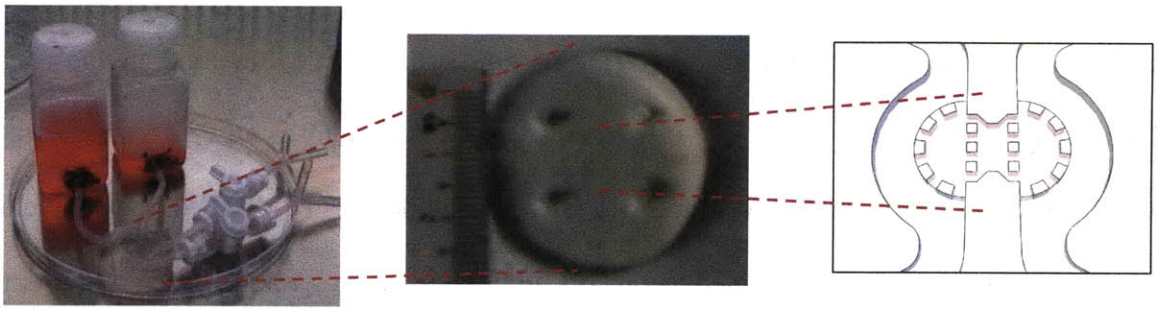

Figure 3: Set-up for applying interstitial flow

3.3. Cell and Device Preparation.

Microfluidic devices were fabricated using soft lithography in a process that has been described previously (7). Polydimethylsiloxane (PDMS, Ellsworth Adhesives, MA) was mixed at 10:1 base: curing agent, poured over a silicon master, and incubated overnight at 80°C. The PDMS was cut from the silicon master, trimmed, and autoclaved in water. The devices were then dry autoclaved and dried overnight in an oven at 80°C. The sterile PDMS devices were then surface activated by plasma treatment for 4min, (Harrick Plasma, Ithaca, NY), coated with Poly-D-lysine (PDL, Sigma-Aldrich, St. Louis, MO) incubated overnight at 37°C, washed with sterile water, and dried overnight at 80°C.

MDA-MB-231 cells originally derived from a pleural effusion were obtained from the American Type Culture Collection (Manassas, VA) and were cultured in standard growth media of 10x DMEM (Invitrogen, Carlsbad, CA) with 10% FBS (Invitrogen). Prior to seeding devices with collagen gel and cells, the devices and a sterile coverslip for each device were plasma treated for 4min in order to ensure a strong bond between the PDMS and coverslip when the device is sealed. Collagen type I (BD Biosciences, Bedford, MA) solution was buffered with 10x DMEM, titrated to a pH of 8.9 with NaOH, and brought to a final concentration of 2mg/ml collagen I in total solution. Cells were harvested with 0.05% Trypsin/EDTA and centrifuged at 12000RPM for 5min. The cells were re-suspended in media at the desired concentration, and the suspended cells were then mixed with collagen I solution to make a final cell density of $2.5x10^5$ or $0.5x10^5$ cells/(ml total solution). The gel-cell solution was added to the devices by hand using a micropipette, and devices were sealed with a coverslip. In order to ensure a tight seal between the PDMS and the coverslip, the gel must be added to the device and the device must be sealed with the coverslip within 30min of plasma treating the device and coverslip. The seeded devices

were placed in an incubator at 37°C for 30min to allow the collagen gel to polymerize before adding media via the surface ports, at a rate slow enough so as not to disrupt the collagen gel. In order to add media without disrupting the gel, it was important to avoid forming a seal between the pipette tip and media port in the device, as pressure used to eject media from the pipette could rupture the gel. A small radius pipette tip (or gel filling tip) was used to wet the glass coverslip at the bottom of the media port, and surface tension drove the media through the media channels on either side of the gel region.

Cells were incubated overnight at 37°C. To apply a pressure gradient, external media reservoirs were connected to the microfluidic chip. The reservoirs were made from modified Nalgene (Thermo Fisher Scientific, Waltham, MA) bottles with Tygon (Compagnie de Saint-Gobain, Paris, France) tubing to connect the reservoirs to the device. Medium was added to each reservoir at volumes that established the desired pressure gradient across the gel. Devices were allowed to reach thermal equilibrium at 37°C before imaging. Valves were added to allow aspiration of bubbles that may form during thermal equilibration, and to prevent media leaking during flow.

Media was supplemented with human recombinant EGF (PeproTech, Rocky Hill, NJ). For CCR7 blocking, human CCR7 MAb (R&D Systems) was added to the media at 5μg/ml.

3.4. Establishing interstitial flow.

After incubating devices with collagen gel suspension bathed in cell media at 37°C and 5% CO_2 overnight, external media reservoirs were attached to the devices. Large reservoirs (12.5cm^2 cross sectional area) were employed so that volume changes due to interstitial flow were less than 0.5% relative to reservoir volume during the course of a 12hr experiment for 3μm/s flow.

3.5. Imaging and image processing.

Phase contrast images were taken every 15min for 16-24hrs in an environmental chamber held at 37°C and 5% CO_2. After imaging, 200nm diameter fluorescent microspheres (Polysciences, Warrington, PA) were added to the media, and fluorescent images were taken to ensure pressure head establishment and flow had not induced gel rupture.

An FEM model was developed in Comsol Multiphysics (COMSOL, Stockholm, Sweden) using an imported Auto-CAD file (Autodesk, CA) of the device geometry. The model determine the fluid velocity vector field by solving Brinkman's equation for flow through a porous media (Equation 3, 12):

$$\mu\nabla^2\underline{v} - \frac{1}{K}\underline{v} - \nabla P = 0$$

Equation 3: Brinkman's equation

Where μ is the viscosity of water, K is the permeability, and P is the pressure drop. The model solved Brinkman's equation for the full 3D geometry of the device in steady state. The permeability was determined experimentally (see Results) and assumed to be constant throughout the region of device with collagen gel. The pressure drop was determined for each experiment by measuring the hydrostatic pressure difference between the upstream and downstream reservoirs.

For cell alignment quantification, images at given time points were segmented using a previously described Matlab (The Math Works) script (13). Another in-house Matlab script fit an ellipse to each segmented cell, and the location of the centroid of each ellipse was passed to Comsol to

determine the local flow velocity vector field. Subsequent vector analysis and quantification was performed using an in-house Matlab script.

For migration quantification, cells were tracked in time-lapse image sequences using the manual tracking plug-in for ImageJ (14, http://rsb.info.nih.gov/ij). An in-house Matlab script determined migration position and velocity vectors from the ImageJ output. The origin of the migration vectors was passed to Comsol to determine the local fluid velocity vector. Further vector analysis, including determining the angle between velocity and migration vectors, was performed in Matlab using an in-house script. Migration data for each cell in one device was averaged over the whole cell population (the number of cells in a population is subsequently denoted by m), and the average migration data for each cell population was averaged over multiple devices (indicated by n). Statistics were tabulated using a one-way analysis of variance (ANOVA).

To quantify the flow field, 200nm fluorescent microspheres were added to the cell media in the upstream reservoir. Microspheres were imaged using fluorescent time-lapse images. Images were binarized using ImageJ, and an automated tracking algorithm in IMARIS (Bitplane, St. Paul, MN) was used to track the beads in the binarized time-lapse images. An in-house Matlab script determined velocity vectors for each bead using the IMARIS output. The origin of each bead was passed to Comsol to determine the local velocity vector. Subsequent vector analysis was performed in Matlab.

4. Results

4.1. System design and geometry

We employed a microfluidic cell culture system to culture cells in a 3D matrix and to subject cells to interstitial flow. The device geometry allows time-lapse imaging to observe the dynamics of the live cell response (Figure 4). The system consists of two channels separated by a region containing single cells suspended in collagen I gel. The region of interest (ROI) imaged during the experiments was the center of the gel region, and only cells located more than 20μm from the PDMS walls were imaged so edge effects could be neglected. The gel dimensions in the ROI were approximately 1.25mm transverse to flow, 0.75mm in the direction of flow and 0.25mm in depth, but sub-regions of 0.5mm by 0.5mm at one depth in the center of the device were imaged to observe the response of cells in 3D matrix, and again only cells located more than 20μm in depth from the PDMS or coverslip were imaged so edge effects could be neglected. These regions contained approximately 10 cells at cell concentrations of 5×10^4 cells/ml and 50 cells at 25×10^4 cells/ml. By applying a hydrostatic pressure gradient across the gel region, a consistent flow field is generated.

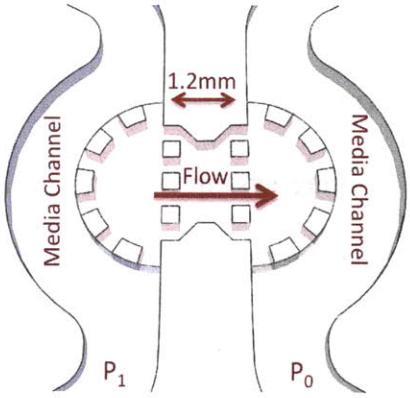

Figure 4: Microfluidic system for seeding cells and applying interstitial flow. Cells are seeded in the central region, and the media channels are connected to external reservoirs to apply a hydrostatic pressure gradient. P1 ad P0 are pressures in the two channels with P1>P0 to generate flow through the gel.

4.2. Interstitial flow field verification

We used FEM software (Comsol Multiphysics) to solve Brinkman's equation for flow through porous medium (12) for our system geometry (Figure 5). Figure 3 shows the central region of the device; the entire device, including the media channels was modeled to ensure accurate computation of the velocity field. Pressure boundary conditions were applied at the inlet and outlet ports of the device. No slip boundary conditions were applied at all PDMS and coverslip surfaces, including central posts. We validated the flow field by adding fluorescent microspheres to the bulk fluid, and we imaged the microspheres using fluorescent time-lapse microscopy (Figure 6).

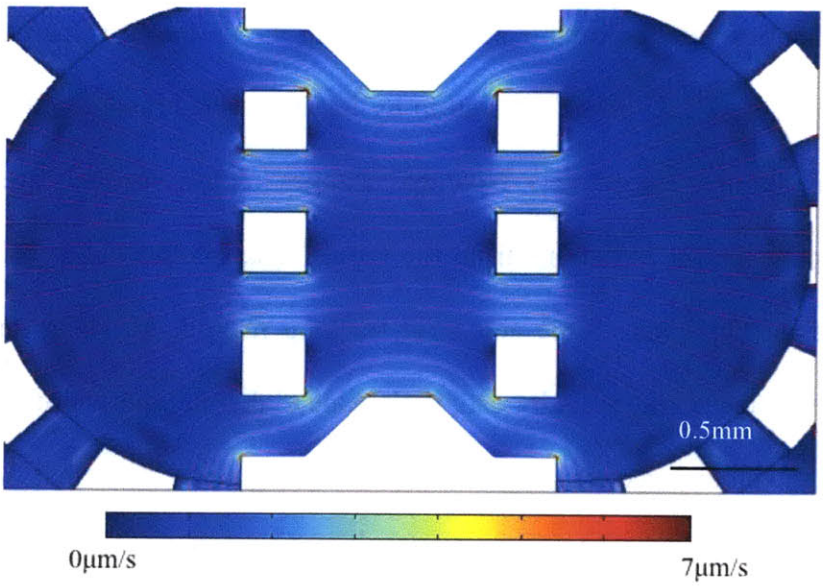

Figure 5: FEM solution of Brinkman's equation in the region of interest for the microfluidic system.

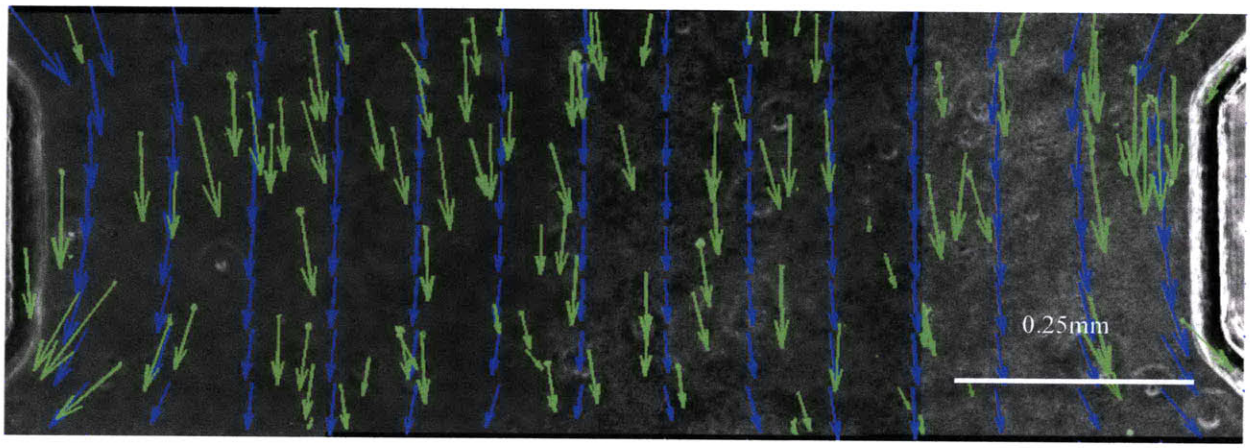

Figure 6: Superimposed fluorescent image of microspheres and phase contrast image of the region of interest in the device. Green vectors indicate magnitude and direction of tracked beads, and blue vectors indicate local predicted magnitude and direction of the flow field from the FEM model.

We found that the measured velocities were repeatable and agreed with the predicted velocities (Figure 7). In what follows, each flow field will be referred to by its respective nominal value, the rounded mean of 0.3μm/s and 3.0μm/s respectively. Note that changes in cross sectional area due to device geometry are responsible for variations from the mean leading to an observable standard deviation in the model velocity magnitude and bead tracking magnitude. However, variation in the magnitude of the bead tracking velocity data is also due to thermal motion of the bead. The measured and predicted velocity vectors were co-directional (Figure 8). Note that the average angle was calculated by averaging the local angle between the model and observed velocity vectors; quantifying the angle in this way allows variation in angle due to device geometry to be neglected. Furthermore, the angle was measured between 0 and 90° so that the average of a collection of randomly oriented vectors would be 45°. Consequently, the variation in angle from the mean leading to the standard error is due to a combination of thermal motion of the bead, nonunifomities in the gel, and experimental error.

Cell responses at 2 different velocity magnitudes, 0.3μm/s and 3.0μm/s, were quantified to sample responses in the range of published *in vivo* values. From the bead tracking data, we determined the hydraulic permeability of 2mg/ml collagen I gel to be $1.55 \times 10^{-13} m^2$, which is similar to previously published values (10, 11).

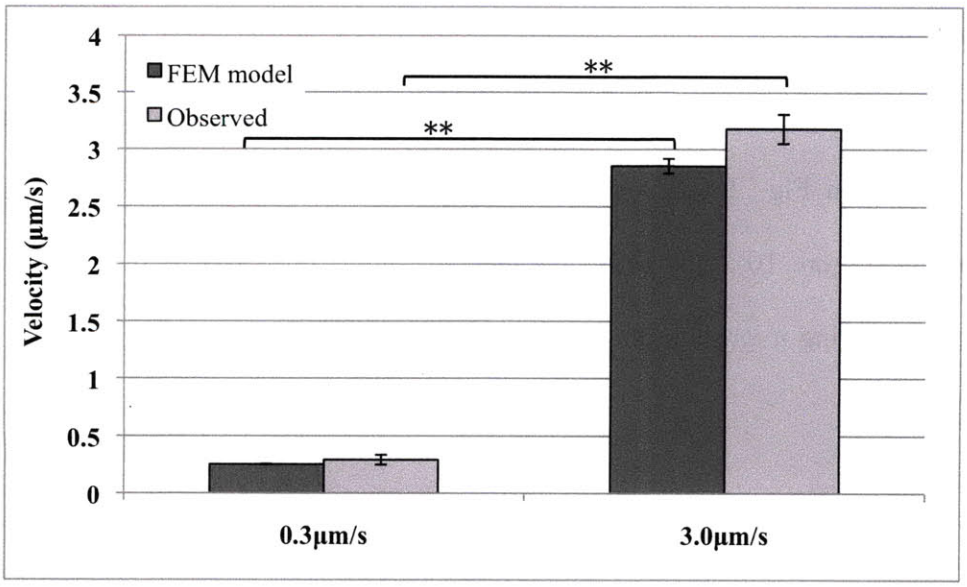

Figure 7: Magnitude of observed velocity and magnitude of velocity predicted by Brinkman's equation. Nominal values are labeled on the x-axis.

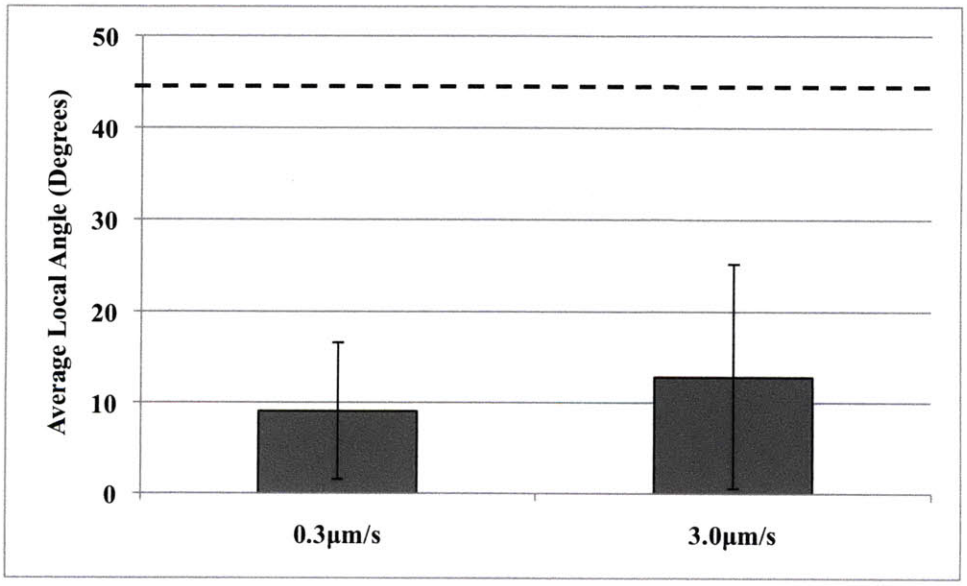

Figure 8: Average local deviation between the measured angle of the velocity vector and that predicted by the FEM. Dashed line indicates average value for a random distribution of angles.

4.3. 3D cell culture

MDA-MB 231 human breast carcinoma cells were seeded in a collagen I gel in microfluidic devices as shown in Fig. 2. The cells were suspended in 3D within the gel (Figure 9) and migrated in 3D (Figure 10). The cells degraded the collagen matrix as they migrated, leaving tracks in the gel during migration, thus suggesting a proteolytically active migration mechanism (Figure 11).

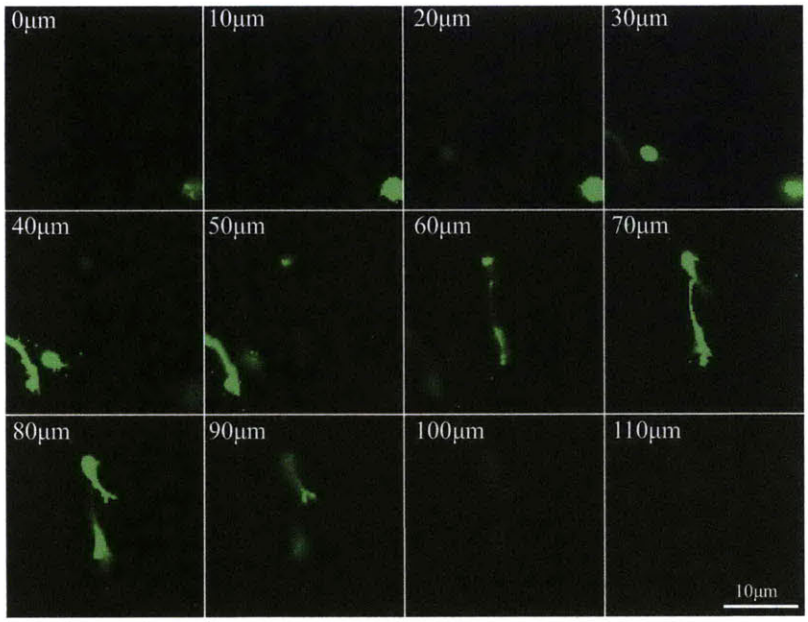

Figure 9: Confocal z-stack (labels indicate height from coverslip) of GFP expressing MDA-MB-231 cells in collagen I gel.

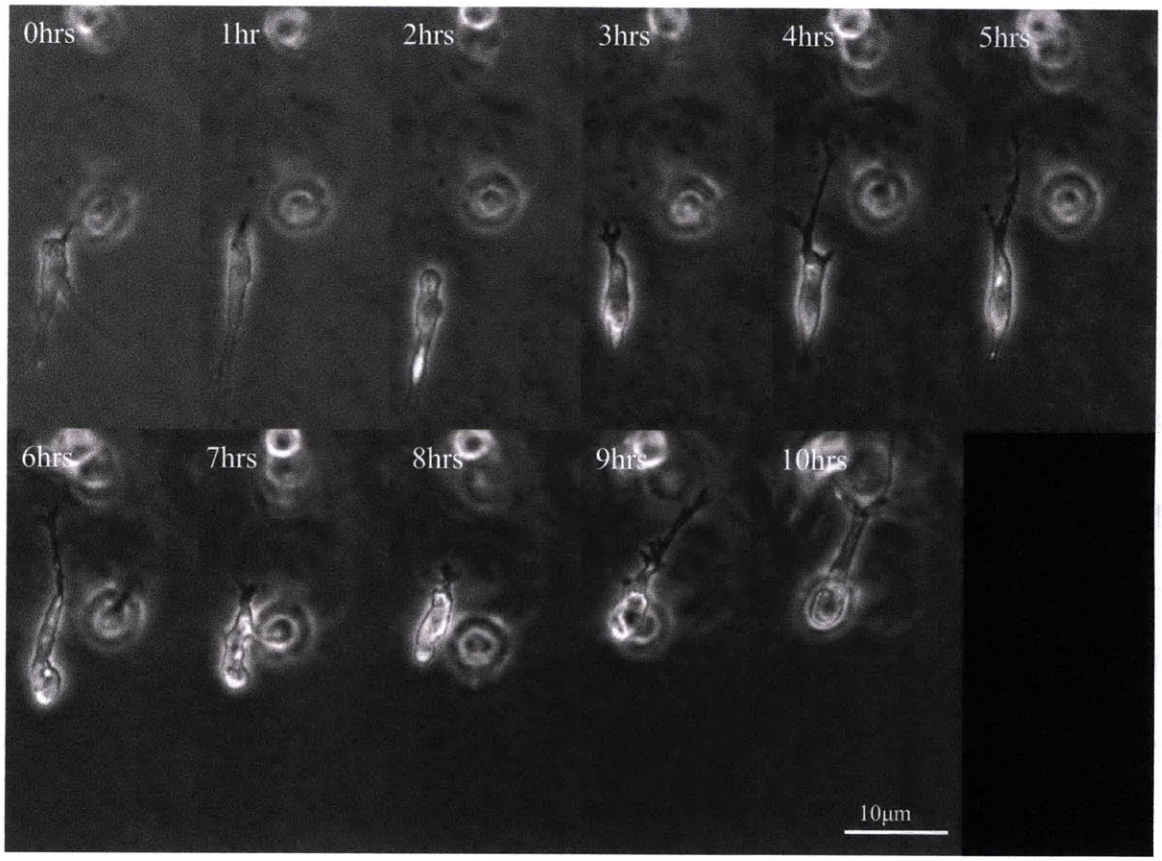

Figure 10: Time lapse images (every 60min) of a cell migrating in 3D in collagen gel.

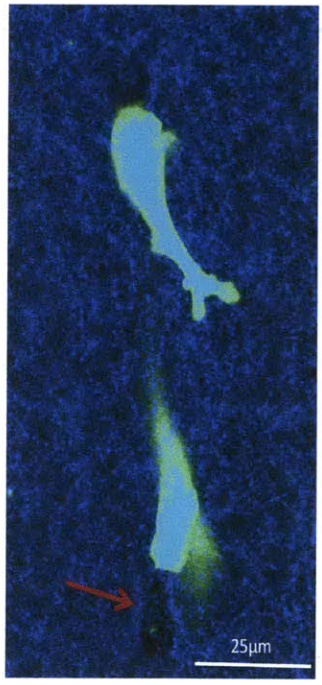

Figure 11: Superimposed confocal reflectance image of cells seeded in 3D collagen I matrix (blue) and confocal image of GFP expressing MDA-MB-231 cells (green). Gap behind cell (red arrow) shows cells migrate in 3D, degrading matrix during migration.

4.4. Cell alignment

When exposed to interstitial flow, cells aligned parallel to flow streamlines (Figure 12a). Figure 10a shows a phase contrast image of cells exposed to 0.3μm/s flow for 12hrs. The blue vectors indicate local velocity vectors as determined by the FEM model. At longer times, cells extended protrusions and subsequently formed multi-cell strings in parallel with the flow streamlines (Figure 12b).

Cell alignment was quantified by measuring the angle between the major axis of an ellipse fit to each cell and the local flow velocity vector from an FEM model of the flow field. After 40hrs, cells exposed to physiologic flow velocities of 0.3μm/s aligned to the streamlines of the flow field with >85% of cells within 45° of the local streamline. Cells not exposed to flow remained randomly oriented with only 50% within 45° of the local streamline (Figure 13 and in all subsequent figures, plots represent mean ±STD, *$p<0.05$, **$p<0.01$ as determined by one-way ANOVA). Without the addition of supplemental EGF, cells did not migrate but still aligned with the flow.

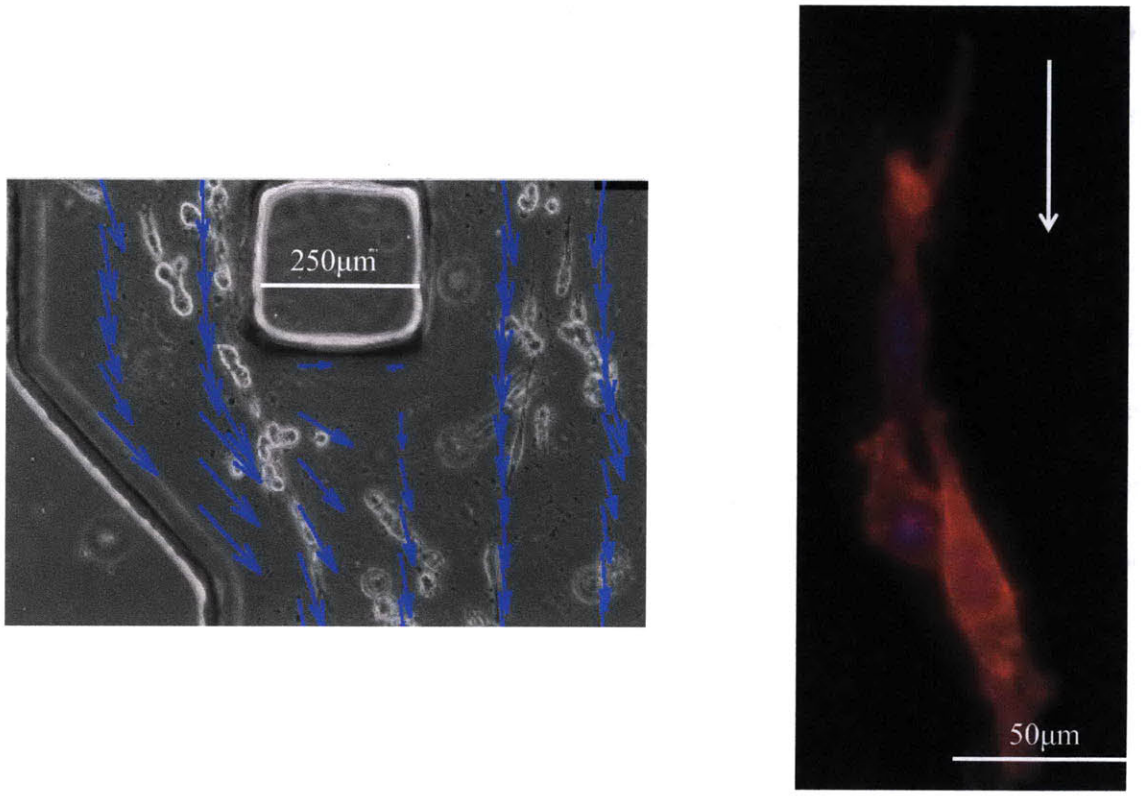

Figure 12: A) Phase contrast image of cells aligned to flow. Flow velocity vectors are overlaid in blue. B) DAPI and phalloidin stain after 36hrs in flow field. Cells form strings after longer times in culture. White arrow indicates direction of flow.

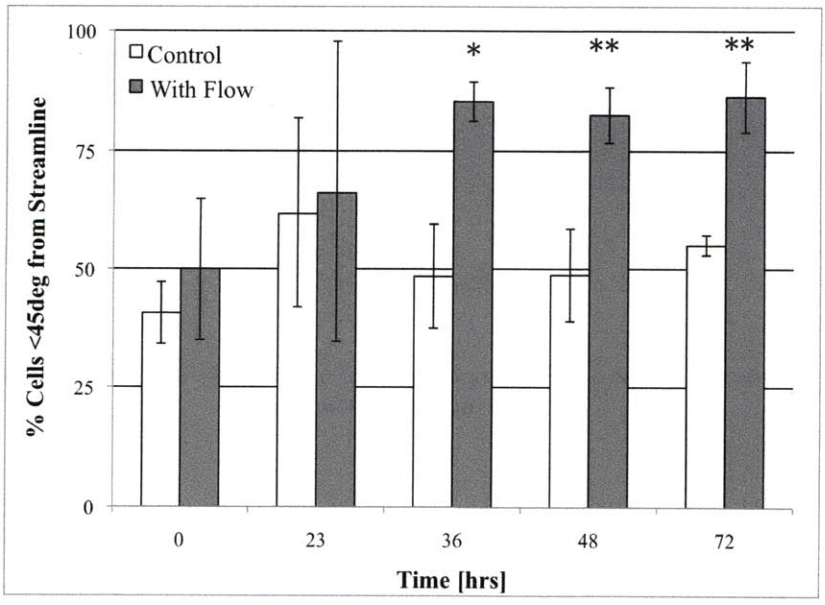

Figure 13: Percent of cell population aligned with flow streamlines. Threshold angle for alignment is 45 degrees.

4.5. Cell morphology

Interstitial flow influenced the morphology of cells suspended in the gel. To quantify these effects in a population, an elongation metric was developed. Elongation is measured as the ratio of the major axis to the minor axis of an ellipse fit to each cell. We then determined the percentage of a cell population elongated more than a threshold value of 2. Interstitial flow increased elongation of cells, but the increased elongation was not apparent until 72hrs after application of flow (Figure 14). This time delay indicates that cells are actively elongating and not being stretched by the pressure drop across the gel.

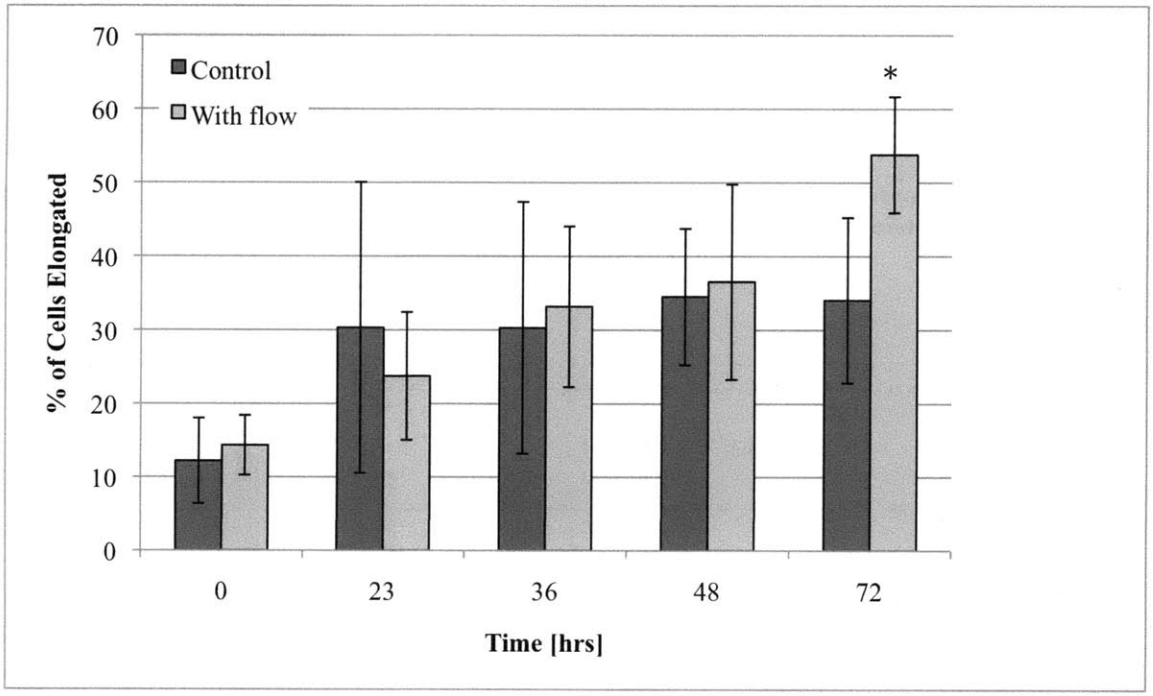

Figure 14: Effect of interstitial flow on cell morphology. Interstitial flow elongates cells, but there is a time delay to increased elongation.

4.6. Cell migration.

Cells were imaged with time-lapse imaging for 16hr intervals, and the center of mass of each cell was tracked. Cell migration velocity was found to be independent of interstitial flow velocity (0.10 μm/s ± 0.05, Figure 15), and cells did not migrate significantly without the addition of supplemental EGF. Cells exposed to interstitial flow migrated with increased directionality, defined as the net migration distance normalized by the total migration distance (0.63±0.073 for 0.3μm/s, 0.61±0.071 for 3.0μm/s, and 0.39±0.071 for control, Figure 16); however, cell migration velocity and motility, defined as the percentage of cells migrating a distance greater than one cell diameter, were unaffected by flow (Figure 17).

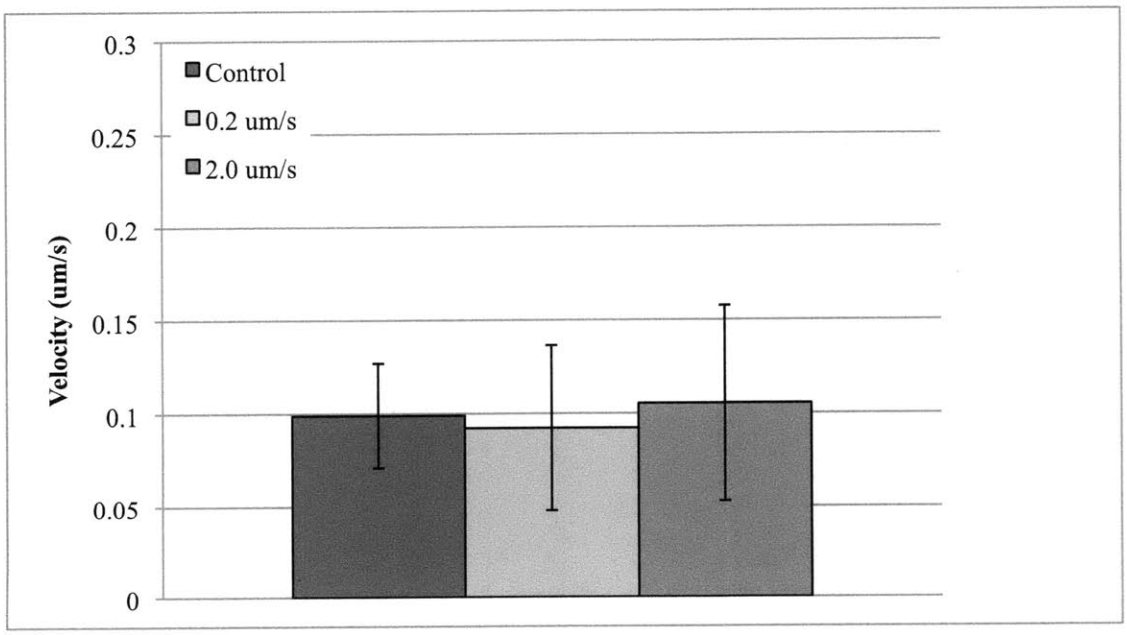

Figure 15: Average migration velocity for cells exposed to flow. Migration velocity magnitude was independent of interstitial flow rate.

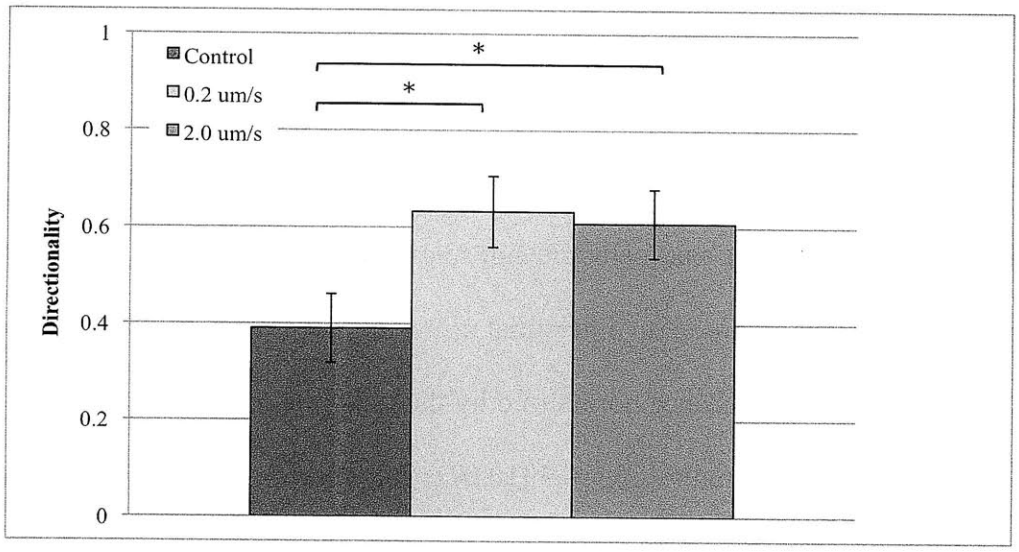

Figure 16: The effect of interstitial flow on average directionality, defined as net migration distance normalized by total migration distance. Cells exposed to flow showed increased directionality.

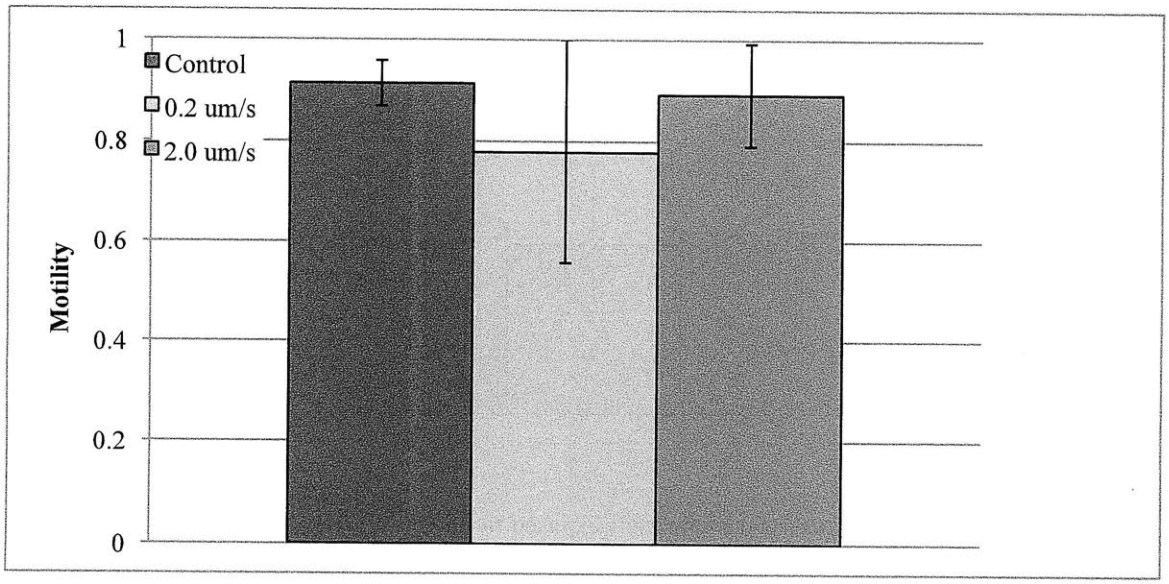

Figure 17: The effect of interstitial flow on cell motility, defined as the fraction of cell population migrating a distance of more than one cell diameter. Motility was not a function of low rate.

4.7. Migration along streamlines.

Interstitial flow induced a directional bias in cellular migration. In Figure 19, sample migration data for a control device and a device with 3.0μm/s flow is plotted on a polar histogram. In devices with flow, cells preferentially migrated along streamlines. To compare migration of cell populations, a metric that scores cells based on direction of migration was developed. The "streamline migration metric" scores cells with a +1 if they migrate within 45° of a streamline and a -1 if they migrate outside of the streamline (Figure 18a). A population has an average score of +1 if all of the cells are migrating on a streamline, score of 0 if as many cells are migrating along the streamline as are migrating perpendicular to the streamline, and score of -1 if all the cells are migrating perpendicular to the streamline. The streamline migration metric is meant to facilitate data visualization and comparison among groups of devices for each experimental condition. However, another metric, fraction of the cell population migrating along streamlines is discussed in the text and plotted in Appendix I. Cells exposed to interstitial flow preferentially migrated along the flow streamlines, with average streamline migration scores of 0.47±0.06 for 0.3μm/s and 0.24±0.04 for 3.0μm/s (Figure 20). These streamline migration scores correspond to 73.6±3.0% and 62.2±4.1% of cells migrating within 45° of streamline, respectively.

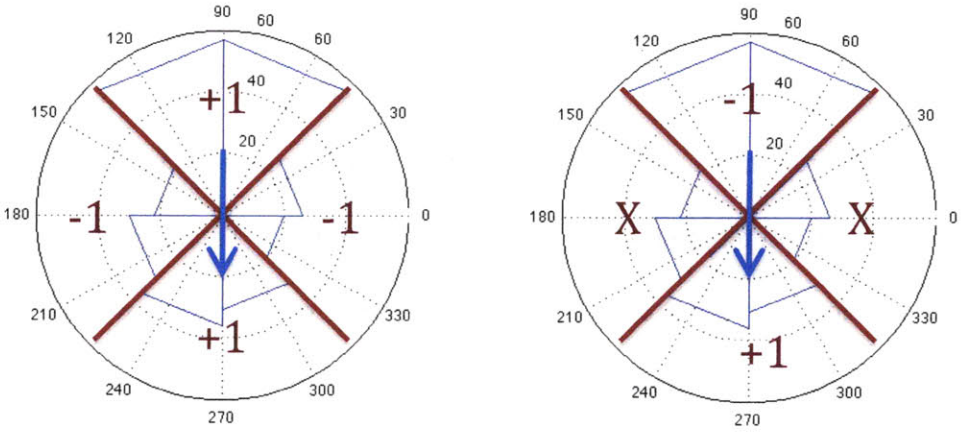

Figure 18: Schematic of scores used to quantify direction of cell migration. Blue arrow indicates streamline. (a) Streamline migration score is used to determine relative population of cells migrating along the streamline. (b) Directional migration score is used to determine bias of migration with or against flow.

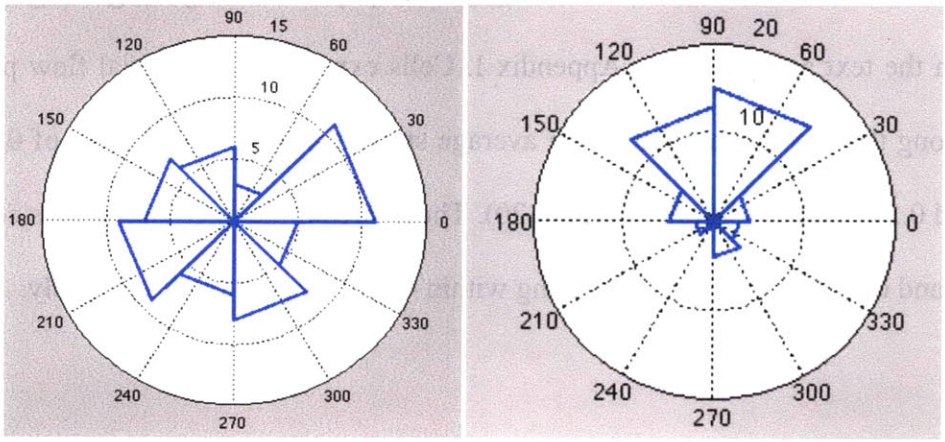

Figure 19: Polar histogram of migration direction for (a) control and (b) cells exposed to 3.0μm/s flow. Flow induced directional bias in migrating cells.

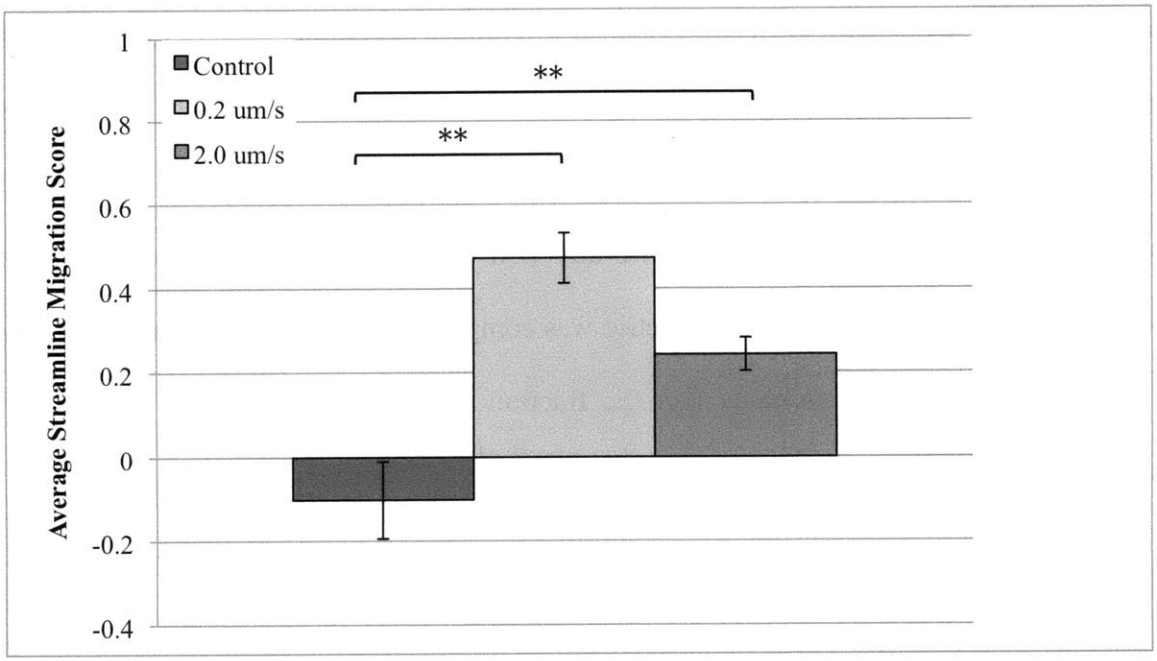

Figure 20: Average streamline migration score for cells exposed to flow. Cells exposed to interstitial flow preferentially migrated along streamlines, although to a lesser extent at the higher flow rate.

4.8. Directional bias along streamlines.

To determine directional bias of migration along streamlines, a "directional migration metric" was computed that scored cells with a +1 if they migrated in the direction of flow and with a -1 if they migrated against the flow (Figure 18b). If a population has an average score of +1, all of the cells are migrating with the flow, and if the population has an average score of -1, all of the cells are migrating against the flow. Of the cells migrating along the streamline, a greater percentage of cells migrated upstream than downstream. The strength of this upstream bias was a function of interstitial flow rate. In an interstitial flow field of 0.3μm/s mean flow velocity, the average

directional migration score was -0.18±0.15, and in a 3.0μm/s interstitial flow field more cells migrated against the flow yielding an average directional migration score of -0.40±0.08 (58.9±7% and 71±4% of cells migrating along the streamline, respectively). Cells in control devices did not preferentially migrate in either direction (Figure 21). As with the streamline migration metric, the directional migration metric was computed to facilitate comparison among many different experimental conditions, but the fraction of cells migrating upstream is also referenced in the text and given in Appendix I.

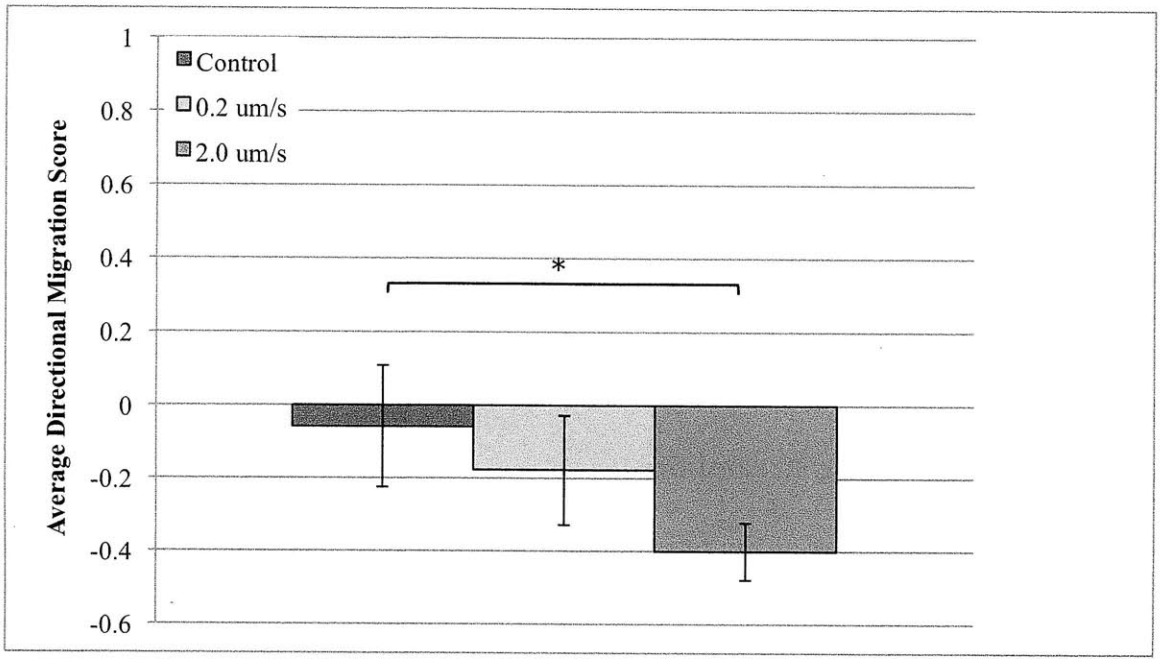

Figure 21: Average directional migration score for cells exposed to flow. Cells at high flow rate show a significant bias for migration in the upstream direction.

4.9. Effect of EGF on migration direction

EGF is added at a uniform concentration immediately after cell seeding, and media in both upstream and downstream reservoirs are supplemented with EGF to prevent the formation of EGF molecular gradients. However, EGF gradients could arise within the gels due to binding of EGF to collagen and upstream cells. To test whether directional bias was due to such an EGF gradient, we saturated the devices with 50ng/ml of EGF. The directional biases of migration were maintained even at this saturating concentration of EGF; the streamline migration score for 10ng/ml EGF was 0.314±0.06 and for 50ng/ml EGF 0.302±0.11, and the directional migration score for 10ng/ml EGF was -0.249±0.07 and -0.250±0.11for 50ng/ml EGF (Figure 22).

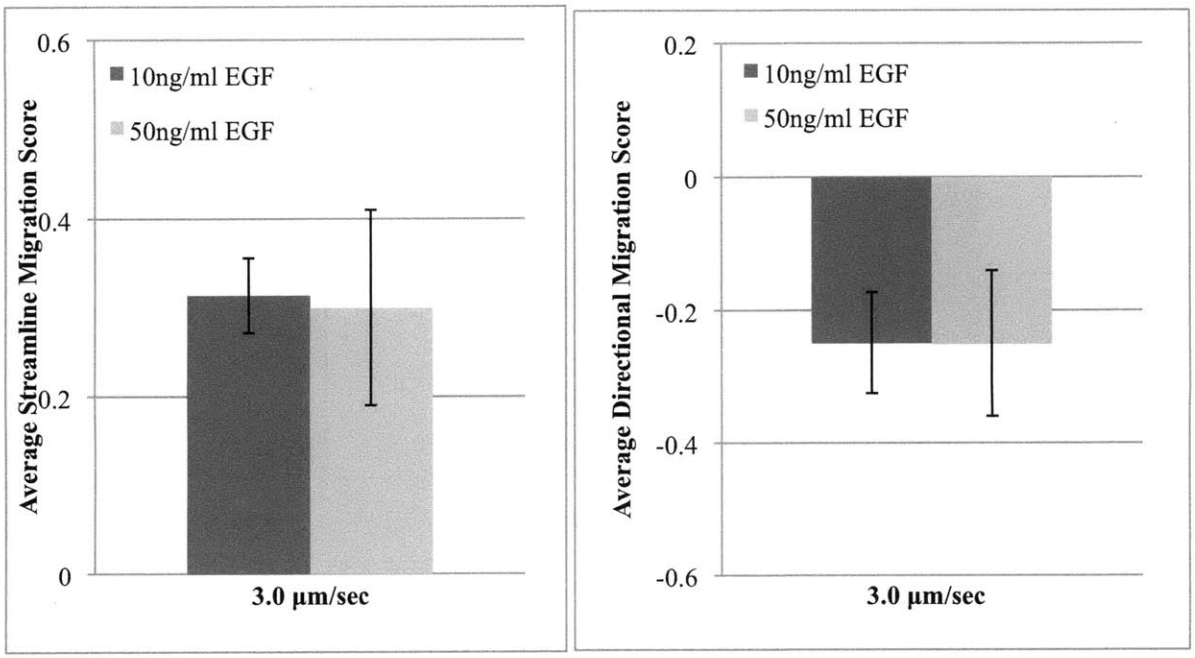

Figure 22: Streamline and directional migration scores for devices at 10ng/ml EGF and a saturation concentration of 50ng/ml. Saturating the devices with EGF did not effect directional bias of cell migration indicating that directional bias is not due to EGF gradients.

4.10. Effect of cell density.

In order to test for the effect of cell density on directional migration under flow, experiments were conducted in the collagen I gels at two different seeding densities, 25×10^4 and 5×10^4 cells/ml. This corresponds to a difference in intercellular distance by a factor of approximately 2. Many of our findings were unchanged as a result of the reduction in cell density. Increasing the intercellular distance did not significantly affect cellular motility (Figure 23) or directionality (Figure 24), and caused a small though not significant decrease in migration velocity (Figure 25).

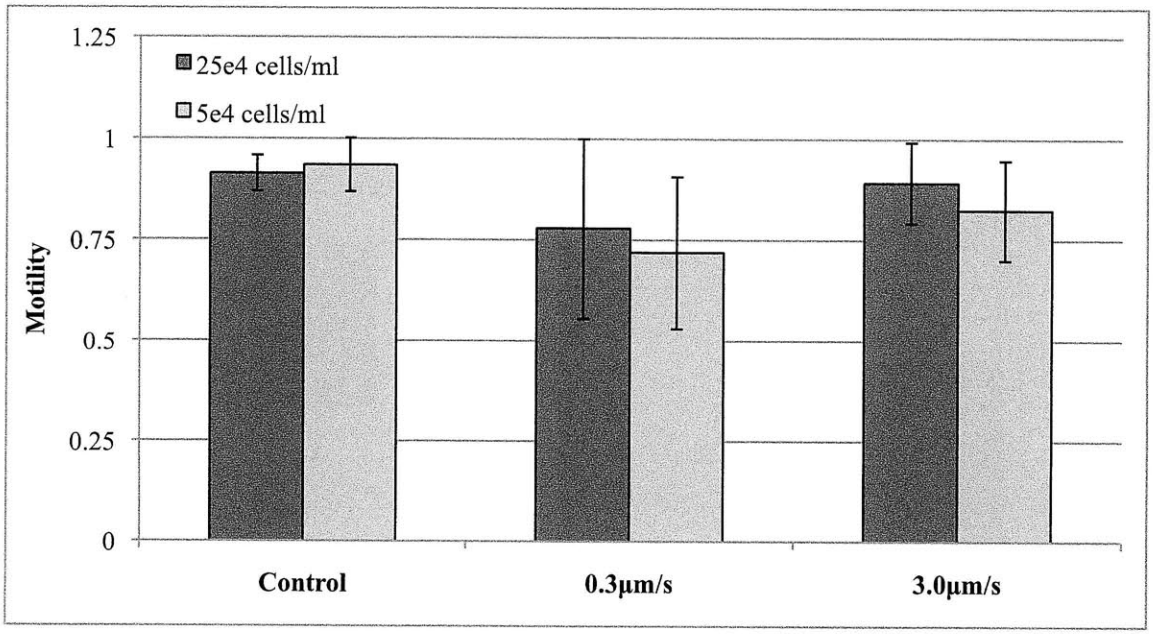

Figure 23: Motility was not a function of intercellular distance

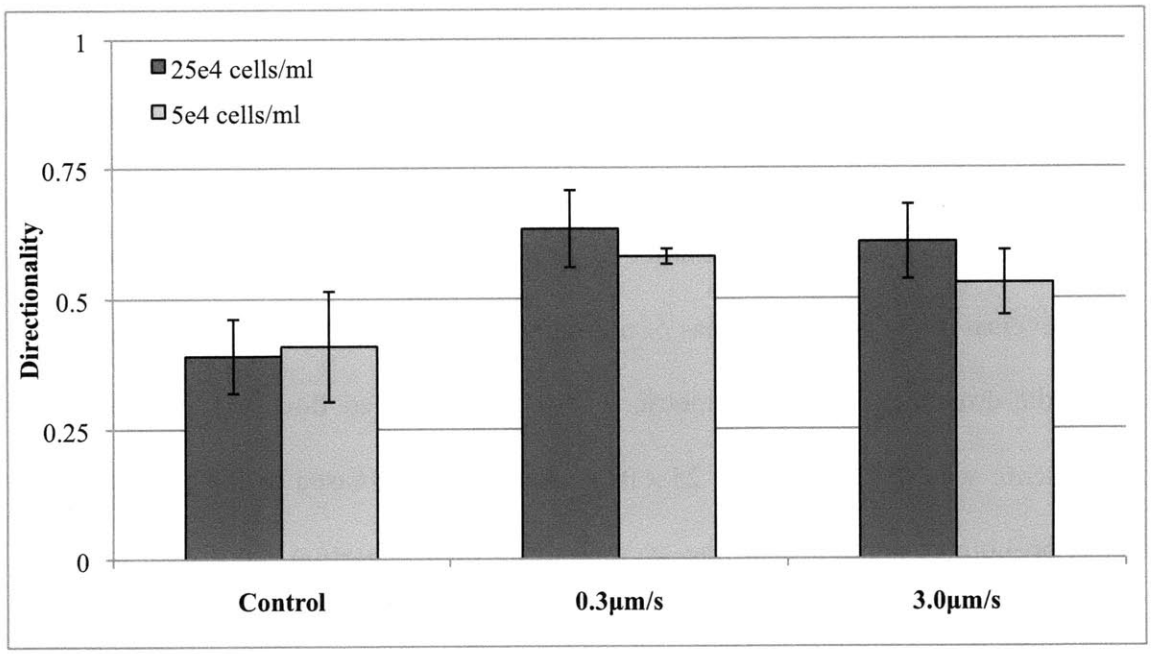

Figure 24: Directionality was not a function of intercellular distance.

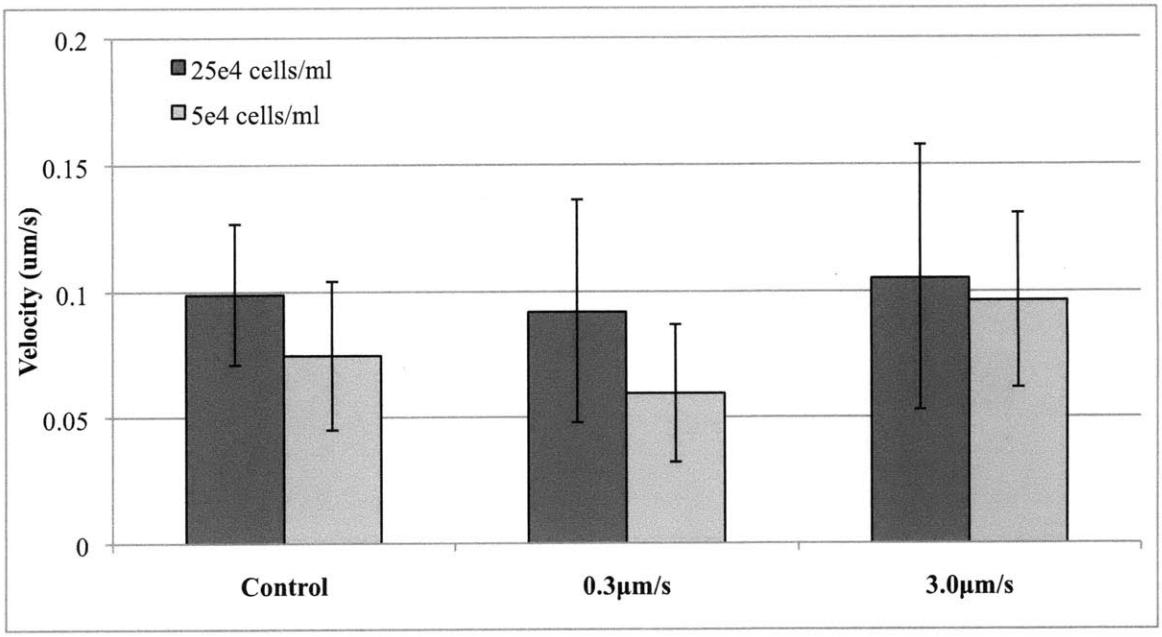

Figure 25: Increased intercellular distance caused a reduction in migration velocity, but the difference was not statistically significant.

Increasing intercellular distance also did not affect the bias toward migration along streamlines in a 0.3μm/s interstitial flow field, although a smaller percentage of cells migrated along streamlines in a 3.0μm/s interstitial field when seeded at a lower concentration (Figure 26). Strikingly, decreasing cell density exerted a dramatic effect on the direction of migration, causing a reversal in the directional bias of migration relative to the flow as indicated by the sign change in the directional migration metric. For 0.3μm/s applied flow, the average directional migration score was -0.177±0.15 at 25×10^4 cells/ml but increased to 0.570±0.18 at 5×10^4 cells/ml. For 3.0μm/s applied flow, the average directional migration score was -0.401±0.08 at 25×10^4 cells/ml but increased to 0.307±0.16 at 5×10^4 cells/ml (Figure 27).

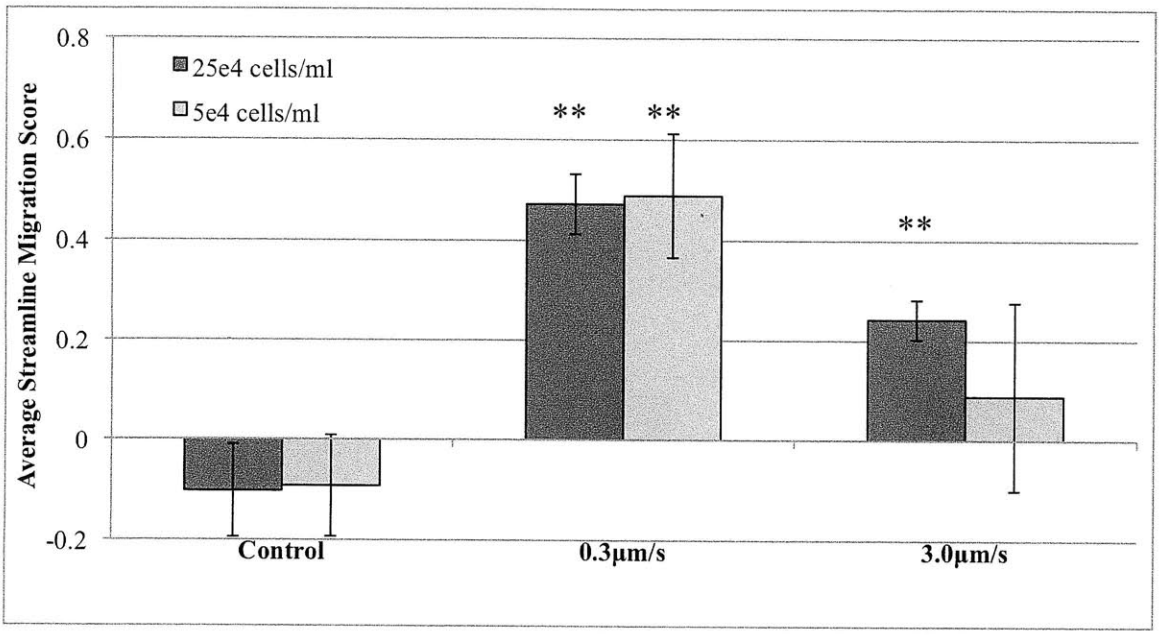

Figure 26: Effect of reducing cell density on migration along streamline. At high interstitial flow rates, increasing intercellular distance decreased biased migration along streamlines.

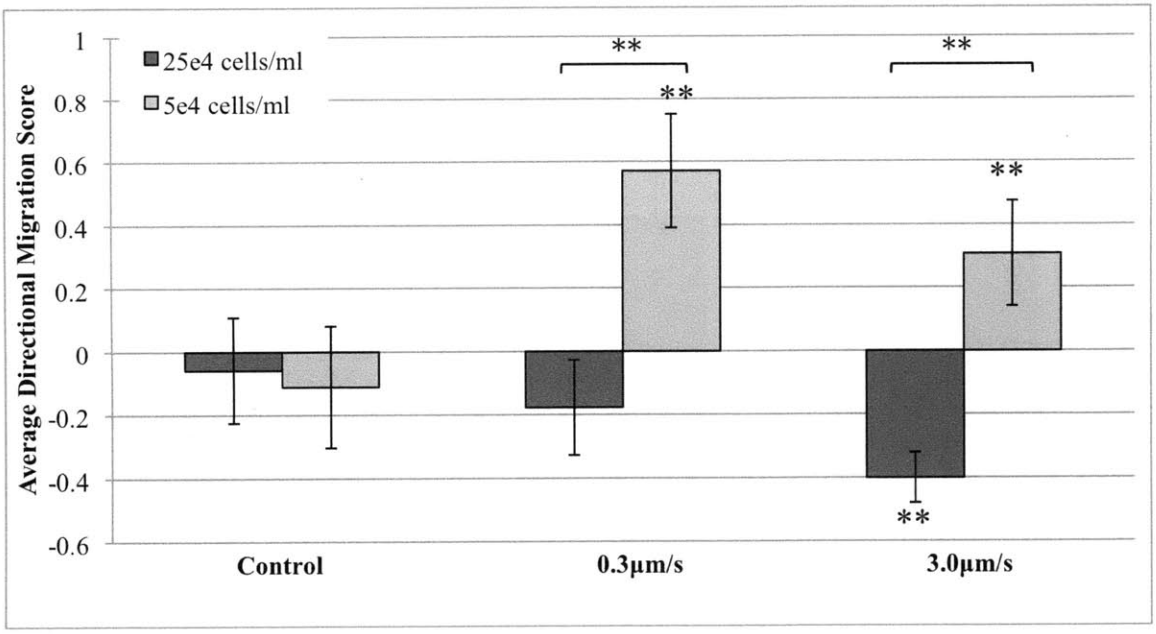

Figure 27: Effect of reducing cell density on directional bias of migration. Increasing intercellular distance caused significant migrational bias in the direction of flow.

4.11. Effect of blocking CCR7 signaling pathway.

Addition of anti-CCR7 blocking antibody caused a significant decrease in motility and migration velocity for cells not exposed to flow; however, interstitial flow recovered this decrease (Figure 28, Figure 29). Blocking CCR7 caused a decrease in directionality of migrating cells, and this effect was pronounced at 0.3µm/s flow (Figure 30). In devices seeded at 25×10^4 cells/ml and subject to 0.3µm/s interstitial flow, addition of CCR7 reduces the bias of migration along streamlines, lowering the average streamline migration metric from 0.472±0.060 to 0.174±0.070, but there is little effect on cells in a 3.0µm/s flow field (Figure 31). At both interstitial flow velocities, blocking CCR7 increased directional migration against the flow (Figure 32).

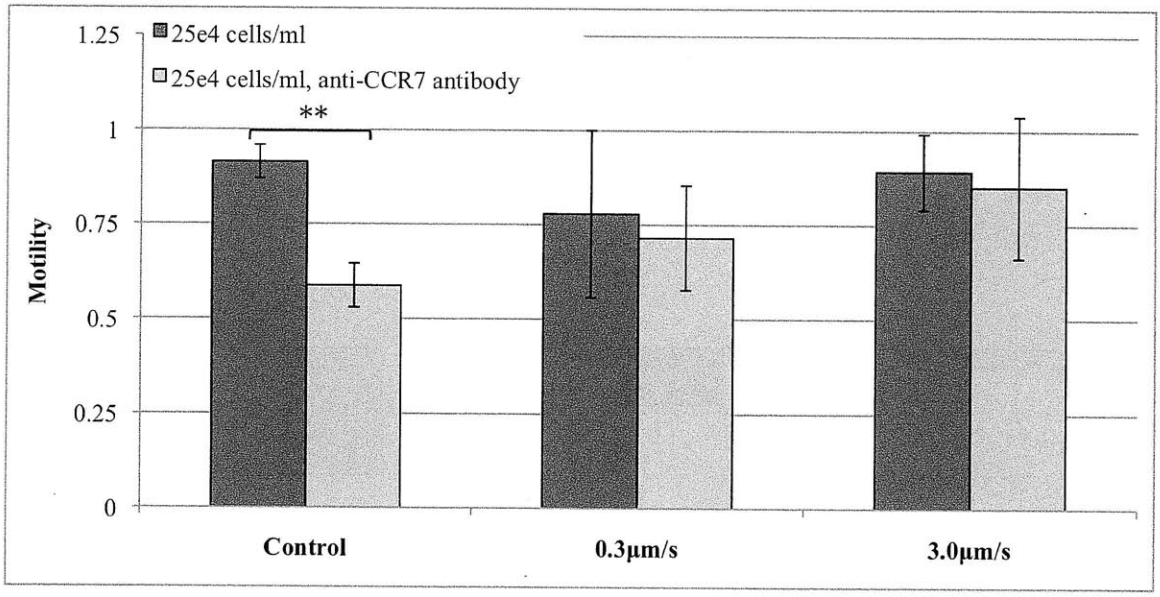

Figure 28: Effect of blocking CCR7 signaling pathway on motility. Blocking CCR7 caused a significant decrease in motility for cells not exposed to flow, but interstitial flow recovered this decrease

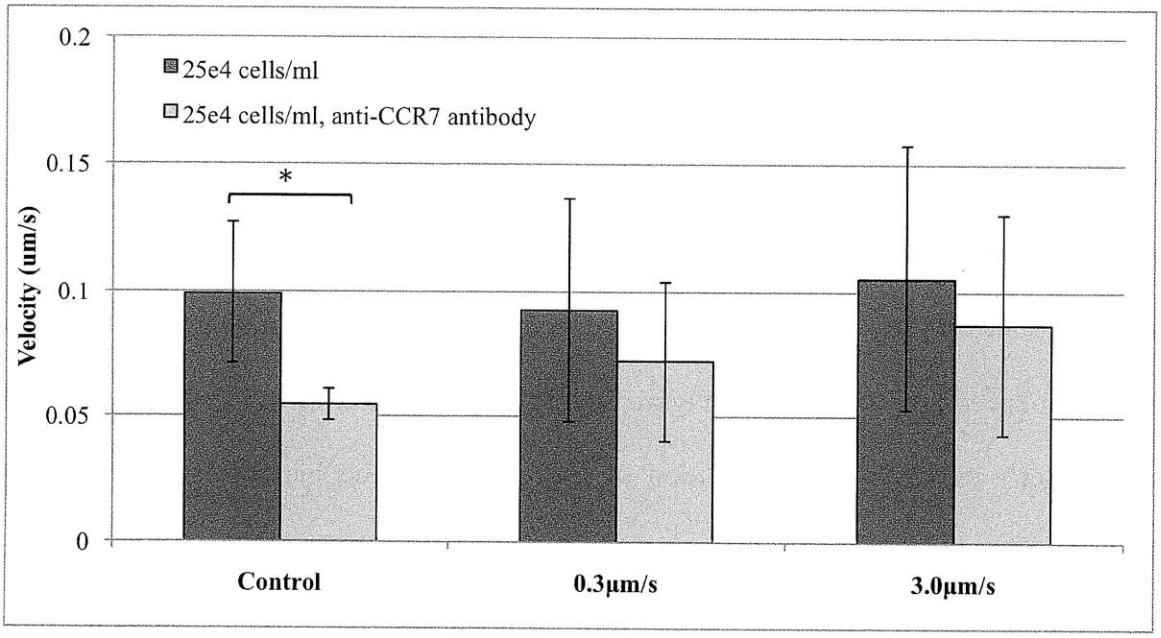

Figure 29: Effect of blocking CCR7 pathway on migration velocity. Blocking CCR7 caused a significant decrease in migration velocity for cells not exposed to flow, but this decrease was recovered in cells exposed to flow.

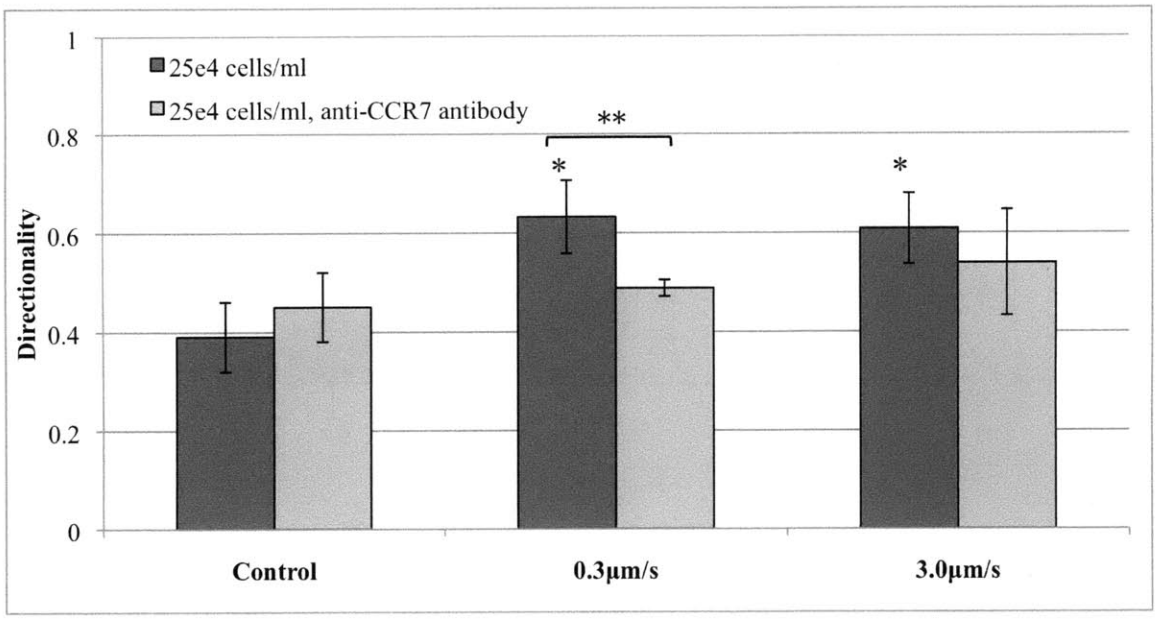

Figure 30: Effect of blocking CCR7 pathway on directionality of migrating cells. Blocking CCR7 caused a decrease in directionality of migration.

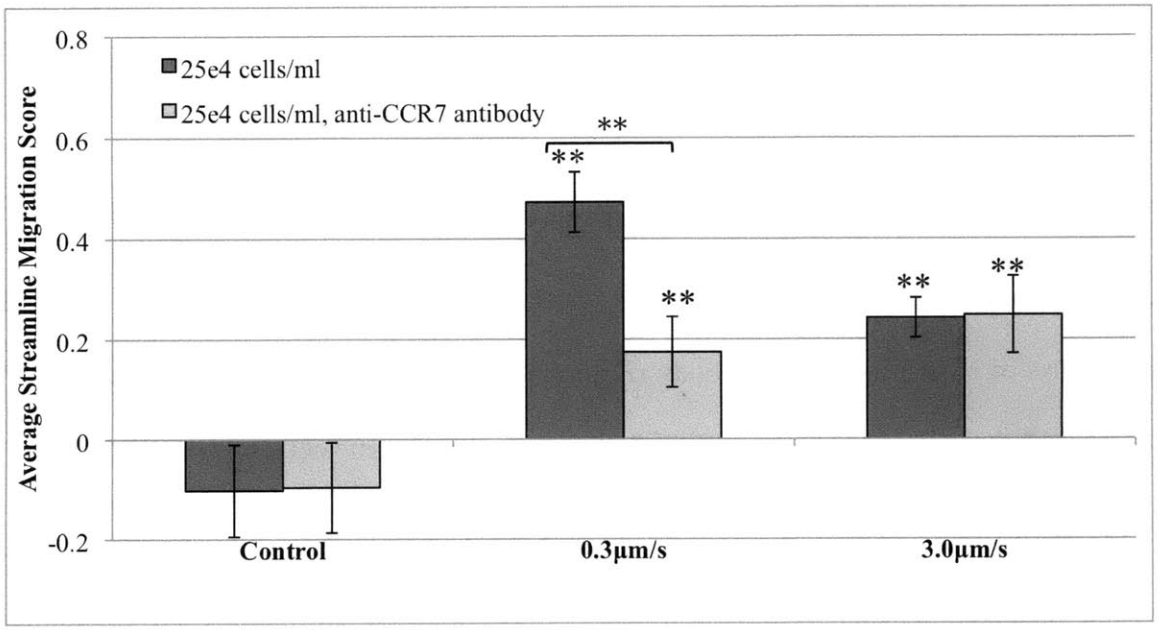

Figure 31: Effect of blocking CCR7 signaling on migration along streamlines. At low flow rates, blocking CCR7 signaling caused a significant decrease in migration along streamlines.

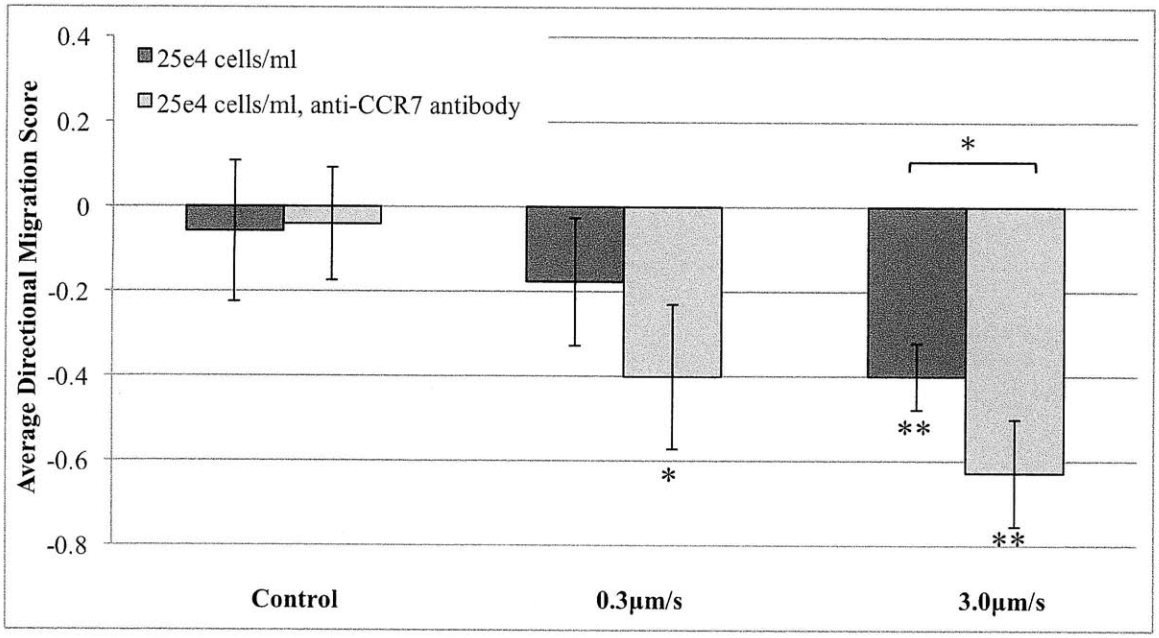

Figure 32: Effect of blocking CCR7 signaling on directional bias of migration along streamlines. Blocking CCR7 caused an increase in directional bias of migration against the flow.

4.12. Effect of blocking CCR7 signaling pathway and reducing cell density.

The decreases in motility and migration velocity observed by reducing cell density are negated with the addition of CCR7 blocking antibody (Figure 33, Figure 34). However, blocking CCR7 further decreased directionality of migrating cells for devices at 5×10^4 cells/ml (Figure 35).

Interestingly, the combined effect of increased intercellular distance and blocking CCR7 resulted in a flow-rate dependent change in migration bias along streamlines. At 0.3µm/s, the streamline migration score was reduced from 0.489±0.122 to 0.201±0.031 with the addition of CCR7 blocking antibody at 5×10^4 cells/ml; however, at 3.0 µm/s, the streamline migration score increased from 0.088±0.188 to 0.384±0.06 at 5×10^4 cells/ml (Figure 36).

In devices seeded at 5×10^4 cells/ml, addition of anti-CCR7 blocking antibody completely negated preferential migration in the direction of flow and in fact, caused preferential migration against the flow. The average directional migration score decreased at both flow velocities, from 0.570±0.12 to -0.420±0.19 at 0.3μm/s and from 0.307±0.16 to -0.649±0.18 at 3.0μm/s (Figure 37).

When comparing cell populations at 5×10^4 cells/ml with CCR7 blocking antibody and populations at 25×10^4 cells/ml with CCR7 blocking antibody, there are no significant differences in directional migration bias. These data suggest that addition of the blocking antibody attenuates the effect of cell concentration on directional migration bias. Furthermore, although the effects are not statistically significant, a consistent trend is observed in the effect of flow rate. At both cell concentrations, increasing the flow rate from 0.3μm/s to 3.0μm/s increases the percentage of cells migrating along the streamline (Figure 38) and increases the upstream migration bias of cells migrating along the streamline (Figure 39).

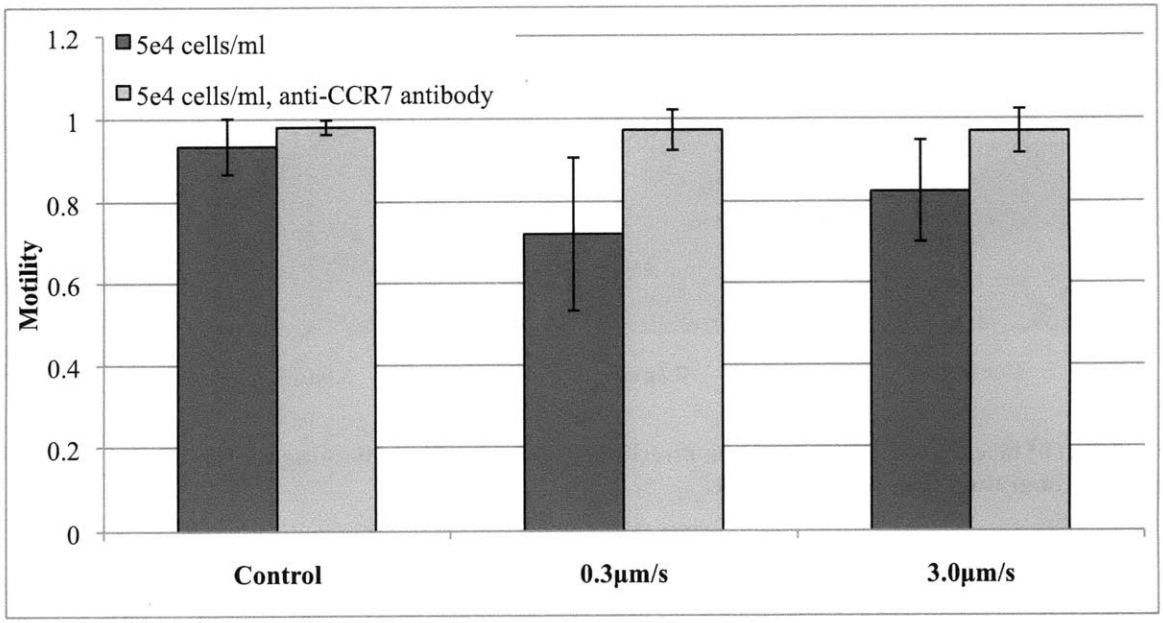

Figure 33: Effect of CCR7 blocking at low cell concentrations on motility of cell population.

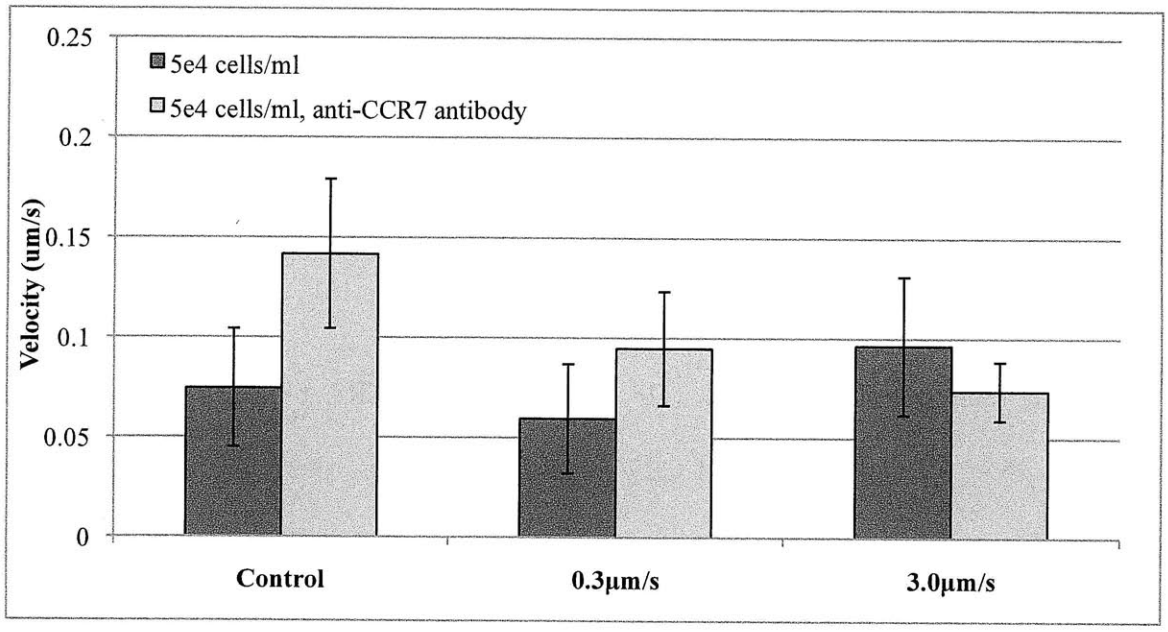

Figure 34: Effect of blocking CCR7 on migration velocity at low cell concentrations

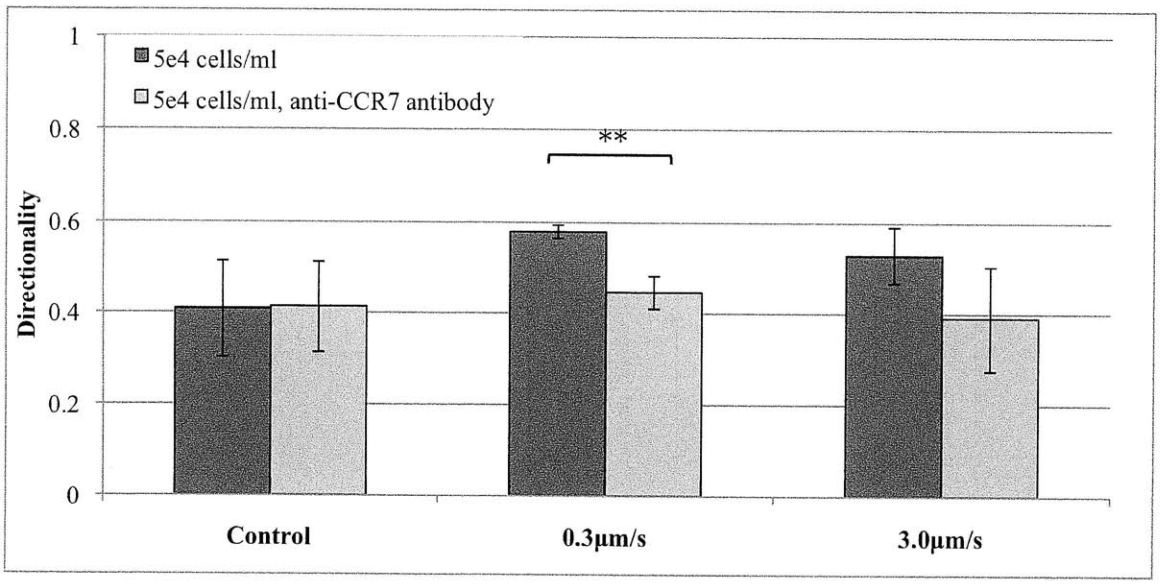

Figure 35: Effect of blocking CCR7 signaling on directionality of migration. Blocking CCR7 reduced directionality of migrating cells exposed to flow.

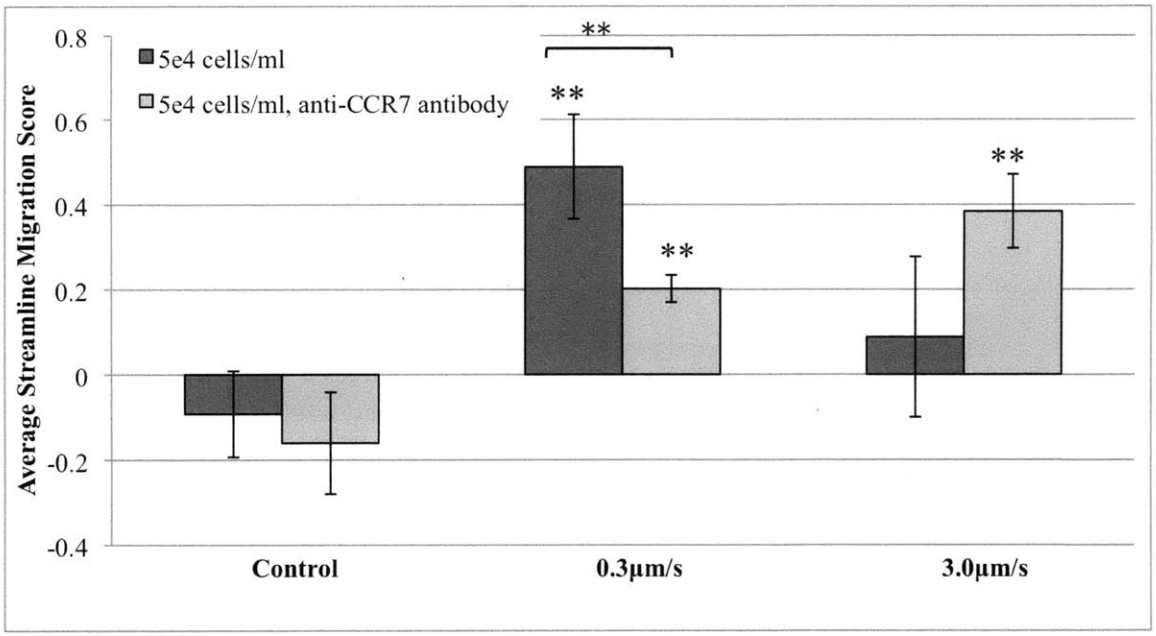

Figure 36: Effect of blocking CCR7 signaling on directional migration of cells.

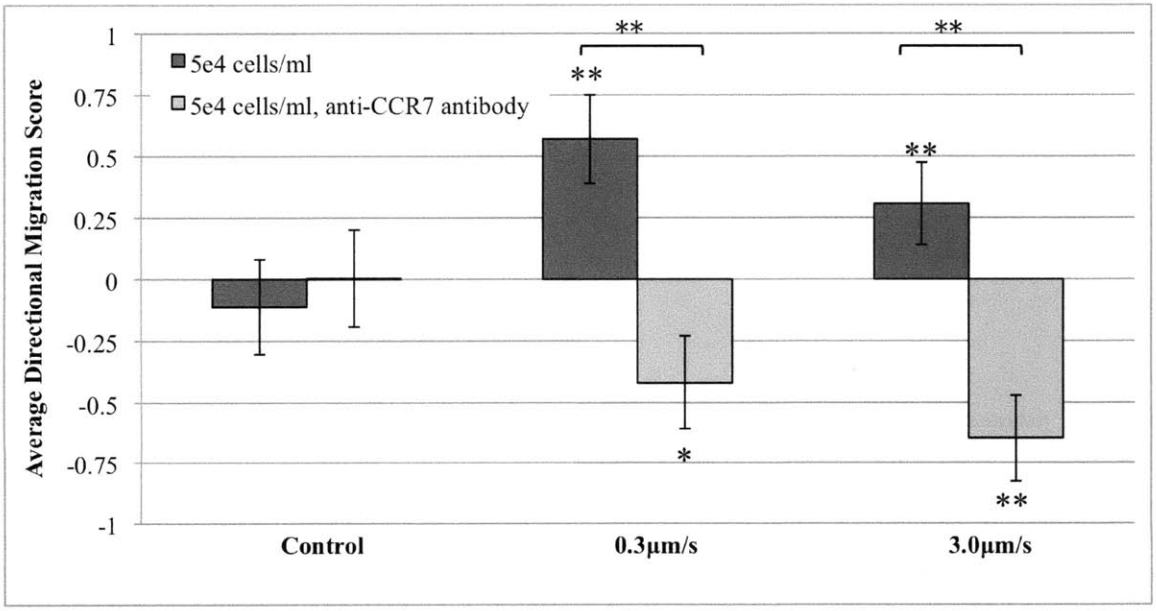

Figure 37: Effect of blocking CCR7 signaling at low cell concentrations on directional bias of migration along streamlines. Blocking CCR7 causes a reversal in directional bias for migrating cells.

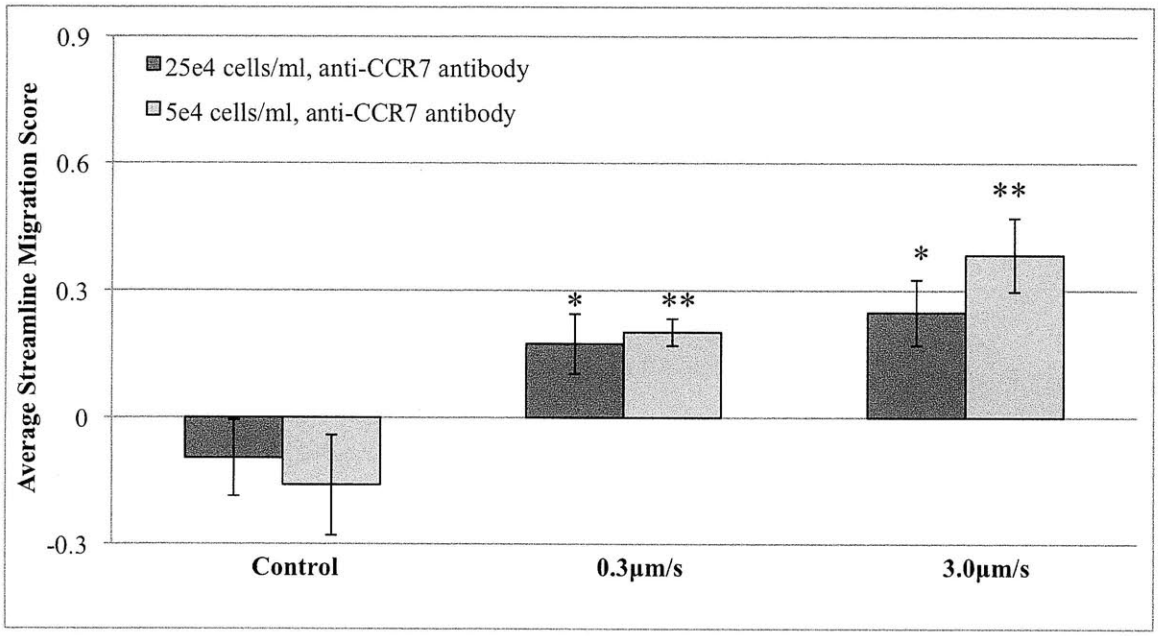

Figure 38: Effect of intercellular distance on directional bias of migration for cells with blocked CCR7 pathways. Intercellular distance does not affect the migration profiles of cells when CCR7 is blocked.

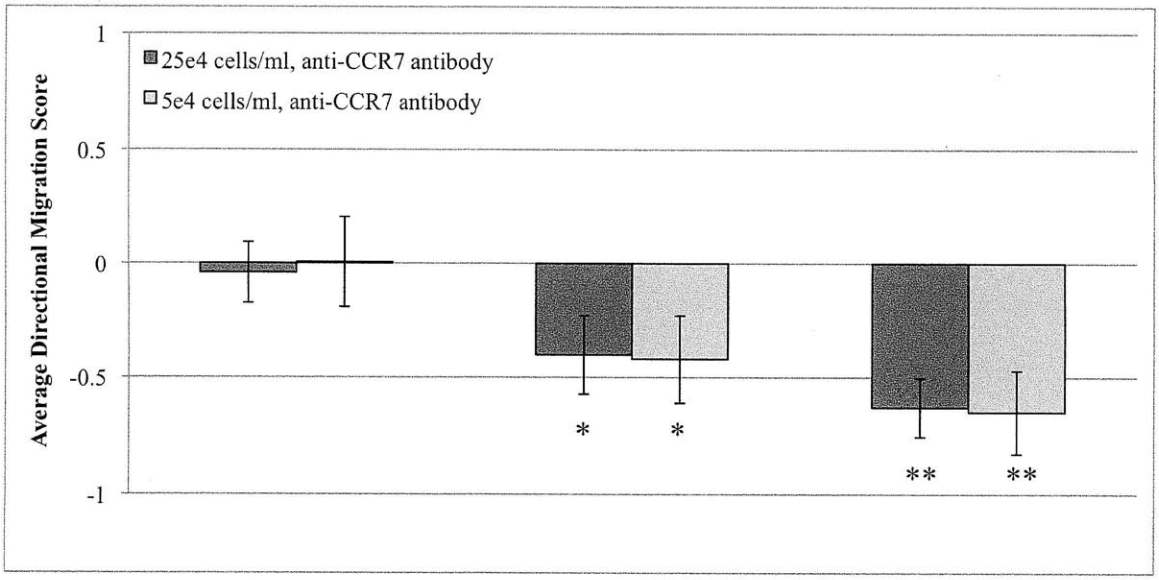

Figure 39: Effect of intercellular distance on directional bias of cells migrating along streamlines. Intercellular distance does not affect directional bias for cells with blocked CCR7 pathways.

4.13. Summary of directional bias in migration

We observed the migration response of cancer cells subject to interstitial flow and identified three parameters that influence the directional bias of migrating cells: seeding density, CCR7 receptor availability, and interstitial flow rate. In the results above, we systematically varied each parameter and observed the migration response, tabulating statistics in a pair-wise fashion when modifying each parameter. Although presenting the data in this fashion allows for rigorous analysis and computation of statistics, the data is overwhelming. In Appendix II, all of the data for average streamline migration and average directional migration scores are presented along with p values from one-way ANOVA between each permutation of the experimental parameters. Figure 42 and Figure 43 (in the Discussion) show trends over all sets of experimental conditions, and the figures are presented to facilitate interpretation of the results.

5. Discussion

5.1. Microfluidic platform

We developed a robust platform for seeding cells in 3D, applying interstitial flow, and observing the cell response in real-time. This platform represents a significant improvement over previous cell culture platforms, most of which were limited to 2D cell culture and do not have the capability to observe time-dependent cell behavior. The Boyden chamber assay, used to develop the autologous chemotaxis model, allowed for observation of increased motility of cell populations, but cells were seeded in an inhomogeneous scaffold and data was collected via end-point staining. We show that interstitial flow induces directional bias in cellular migration, and analysis of this directional bias necessitates observation and quantification of time-dependent cell dynamics. Our platform allowed easily repeatable quantification of these transient cell responses. Furthermore, *in vivo* tumor cells migrate in 3D through an ECM, and our platform provided more physiologic relevance than previous systems as cells were seeded in a 3D scaffold of a reconstituted ECM component. The geometry of the device allowed for modeling of the applied interstitial flow velocity field, and the bead perfusion assay provided verification that the modeled field well approximated the experimentally applied velocity field. Furthermore, our fabrication protocol for the platform allows the potential for high-throughput assays in future experiments.

5.2. Cell alignment

Cells exposed to flow aligned to the interstitial flow streamlines and elongated parallel to the streamlines. The time delay between application of flow and elongation (Figure 14) demonstrates that cells are not stretched by pressure-induced strain on the collagen gel. Furthermore, data from reflectance confocal images demonstrates that cells reorganize the local matrix over time when

exposed to interstitial flow. These data provide evidence that interstitial flow provides a stimulus to cells that results in active cellular reorganization resulting in the alignment of cells. Cells extend protrusions in the direction of flow and eventually form series of elongated cells even when the cells do not migrate. These data demonstrate that a directional stimulus is present even in the absence of migration stimulus and suggest that EGF gradients are not responsible for the directional stimulus, since EGF gradients induce migration *in vitro*. That EGF gradients are not responsible for directional stimulus is supported by experiments where the devices are saturated with EGF (Figure 22).

These elongation data and the formation of cell strings are interesting in the context of collective cell migration. Friedl et al. has observed *in vivo* that breast cancer cells under specific conditions will migrate as a collective front, rather than as individual cells. They demonstrated that migrating cells provide migration-inducing signals and directional cues to cells in the primary tumor (38). Our data provide evidence that interstitial flow may play an important role in this cell-cell signaling.

5.3. Effect of interstitial flow on cell migration

When culture media is supplemented with EGF, cells migrate in 3D. Previous 2D cell culture experiments have demonstrated that EGF is required for cell migration; however, the cell migration velocities we observed are smaller in magnitude than previously published migration velocities for cells cultured in 2D. In 3D culture, cells must degrade the matrix or squeeze through pores in the matrix in order to migrate. Confocal reflectance microscopy data and live cell imaging provide evidence that cells degrade the matrix as they migrate in our culture system, and this matrix degradation is likely responsible for smaller migration velocities.

Interestingly, cell migration velocity did not vary with exposure to interstitial flow. This data, in conjunction with the elongation and alignment data where cells sensed and responded to interstitial flow while not migrating at all, is consistent with previously published data investigating EGF as a chemokine. Wang et al. showed that migration velocity magnitude was a function of bulk EGF concentration and that EGF gradients influenced the directionality of cell migration, but the strength of the gradient did not affect migration velocity magnitude (61).

5.4. Effects of interstitial flow on direction of cell migration

Interstitial flow increases the directionality of cell migration. Directionality, as the ratio of net displacement to total displacement, is a measure of how straight a cell migrates, and a directionality of 0 implies random cell migration while a directionality of 1 represents a straight trajectory. Previously published work has demonstrated that exposure of cells to a chemokine gradient increases the directionality of cell migration (61). Increased directionality results in larger net displacement for migrating cells. Consequently, our data on directionality gives evidence that interstitial flow acts as a stimulus for direction of migration and effects the net displacement of migrating cells.

Interstitial flow does not affect the motility of cell populations, but we found motility is a function of EGF concentration. This seems to violate the finding of Shields et al., who demonstrated that interstitial flow increases the percentage of cells migrating through a membrane in a Boyden chamber (5). However, our live-cell imaging and migration vector analysis helps to rectify this discrepancy. We show that although the total percentage of cells in a population migrating greater than one cell diameter is unaffected by interstitial flow, the percentage of cells migrating along streamlines increases with interstitial flow (Figure 20).

Consequently, if a membrane were placed in our device transverse to the flow direction, we would observe a higher percentage of cells migrating through the membrane since the normal vector of the membrane would be parallel to the streamlines. Counting cells that migrate through the membrane is effectively how Shields et al. quantified motility in the Boyden chamber. Our 3D culture system has allowed us to visualize the dynamics of the cell response to interstitial flow and to contribute new insight into time-dependent cell dynamics, such as direction of cell migration, which build upon previous models such as autologous chemotaxis.

5.5. Cellular transport environment with interstitial flow

Molecules, such as chemokines, secreted by a cell exposed to interstitial flow are transported by convective fluid flow. Understanding how convective flow distributes ligands and the resulting concentration fields are crucial to investigating flow-induced cellular migration stimuli. Equation 2 gives the expression for the Peclet number, a non-dimensional number that compares the relative magnitude of diffusive transport and convective transport. Fleury et al. proposed, in the context of autologous chemotaxis, that the Peclet number (Pe) is crucial in autocrine signaling, and that higher Pe results in larger transcellular autocrine gradients (8). The reported diffusivity for CCL21 is 130$\mu m^2/s$, and the length of cells in the direction of flow is about 25μm. Consequently, the Pe for 0.3μm/s flow is 0.06, and the Pe for 3.0μm/s flow is 0.6. Each of these values is less than 1, so transport is diffusion dominated, but each flow rate represents a significantly different transport regime. Using an FEM model, Fleury et al. showed that a transcellular gradient of 11%, concentration at the downstream side of the cell normalized by concentration at upstream side, can result for CCL21 about single cells at Pe 0.05, but a gradient of >133% can result at Pe 0.5 (Figure 40). Transcellular gradients of ligands that bind to cell surface receptors can lead to differential receptor binding, with more bound receptors

downstream than upstream. Differential receptor binding for certain receptors, such as CCR7, can induce directional migration (62). Therefore, we expect the range of Pe in our experiments to provide insight into the role of convective transport in guiding cell migration.

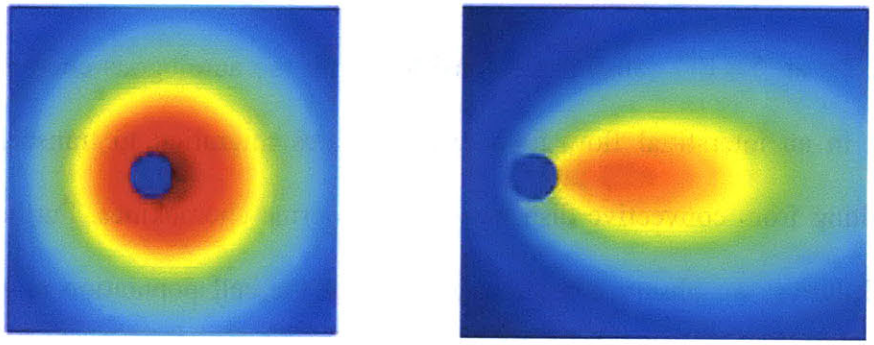

Pe = 0.05 **Pe = 0.5**

Figure 40: Effect of Peclet # on transcellular distribution of autocrine morphogens. Flow is from left to right. Plotted is normalized concentration, red is maximum and blue minimum concentration. Adapted from Fleury et al. (8).

5.6. Autologous chemotaxis

In devices seeded at 5×10^4 cells/ml, cells preferentially migrated along streamlines and in the direction of flow. At this low cell concentration, the distance between cells is on average 170μm while cell diameters are on average 25μm. We expect the magnitude of transcellular autocrine gradients to be a function of cell density. When cells are in close proximity, ligands secreted by neighboring cells will influence autocrine concentration fields. However, at low cell density, we expect less of an effect of neighboring cells on autocrine gradients due to the larger distances between cells.

Figure 41 demonstrates the effects of cell density on autocrine gradients. In Figure 41a, the distance between cells is greater than twice the cell diameter and clear autorine gradients can be

observed. In Figure 41b all parameters and boundary conditions governing transport are the same as in Figure 41a but the distance between cells has been halved. The resulting concentration field local to the central cell in Figure 41b demonstrates that the overlapping autocrine and paracrine fields dissipate the autocrine transcellular gradient.

Our data for cells at 5×10^4 cells/ml are consistent with the autologous chemotaxis model for cell migration in an interstitial flow field, which relates migration to transcellular autocrine gradients resulting from convective distribution of autocrine chemokines. Furthermore, at flow velocities of 3.0μm/s, we observed a larger fraction of the cell population migrating with the flow than the fraction we observed at 0.3μm/s. We hypothesize that this effect of flow rate is due to larger transcellular autocrine gradients characterized by the larger Pe discussed above.

Shields et al. identified the CCR7 chemokine receptor as the key receptor in the signaling pathway responsible for autologous chemotaxis (5). When we blocked CCR7 with blocking antibody, migration bias in the direction of flow was attenuated. Furthermore, when CCR7 was blocked, cell density did not affect bias of migration direction at each flow rate. These data support and extend the autologous chemotaxis model to demonstrate the effects of autologous chemotaxis on directional migration.

Autologous chemotaxis has been presented only in the context of its effects on net migration of a population of cells, and support for interstitial flow inducing autocrine transcellular gradients has been limited to end-point fixed staining of CCR7 receptors on cells exposed to flow (5). However, with our experimental platform, we are able to demonstrate that autocrine gradients influence the migration direction bias of cells exposed to interstitial flow. Furthermore, the

CCR7 blocking experiments support the hypothesis that the CCR7 receptor is responsible for sensing the autocrine gradients and stimulating downstream migration.

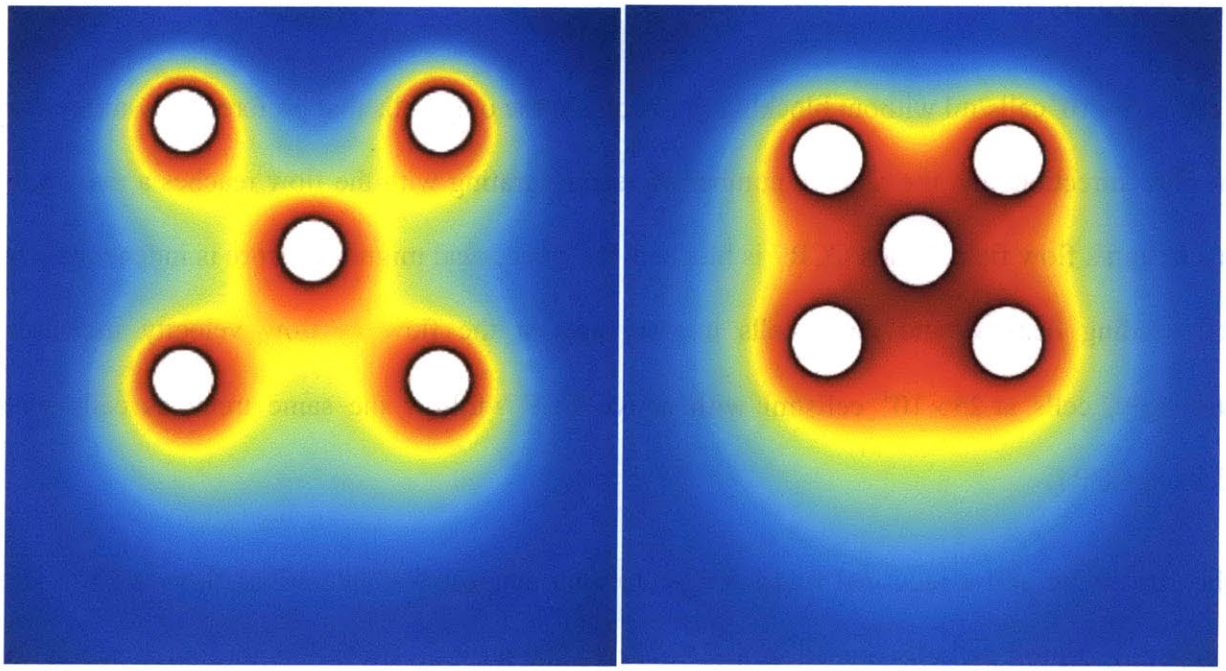

Figure 41: Transport model for demonstrating the effect of cell density on transcellular autocrine chemokine gradients. Normalized concentration, with red maximum concentration and blue minimum concentration. All parameters are the same in both figures, except intercellular distance.

5.7. Competing signals.

In Figure 42 and Figure 43 we present the average streamline migration score and average directional migration score for each combination of the experimental parameters. Error bars are omitted for clarity but have been presented in the Results and in Appendix II. Plotting the data in this fashion allows for observation of trends in the data that are not apparent from pair-wise comparison.

Without CCR7 blocking, the streamline migration score reaches a maximum at 0.3μm/s, but interestingly, we do not see the peak when CCR7 is blocked. Furthermore, the streamline

migration score increases with flow rate when CCR7 is blocked. Although there are slight differences in magnitude, the trends of the curves with and without CCR7 antibody are independent of cell density.

Cells at 5×10^4 cells/ml without blocking antibody are the only cells that preferentially migrate in the flow direction, and the relative number of cells migrating with the flow reaches a maximum in a 0.3μm/s flow field. When CCR7 is blocked, the directional migration score is independent of cell seeding density, and more cells migrate against the flow as flow velocity increases. Strikingly, cells at 25×10^4 cells/ml with active CCR7 follow the same trend as cells with blocked CCR7.

The streamline and directional migration score data suggest that interstitial flow imparts two competing stimuli on cells seeded in a 3D matrix. The positive streamline migration scores for cells at low seeding density and without antibody suggest that one of these stimuli is CCR7 dependent and drives cells in the direction of flow as suggested above. Furthermore, the difference in directional bias for cells seeded at at 5×10^4 cells/ml and 25×10^4 cells/ml suggest that the anti-CCR7 ligand is an autocrine chemokine. These data support the autologous chemotaxis model of Swartz et al.

We hypothesize that a second signal drives upstream migration and competes with CCR7. Because upstream migration persists at low cell density and low flow rates when CCR7 is blocked we hypothesize that the second signal is also an autocrine signal. However, unlike the CCR7-dependent downstream migration, the second signal increases in strength with increasing fluid velocity, and furthermore, the strength of the second signal is cell density independent. These data suggest that the mechanism competing with CCR7 is unaffected by concentration

fields of neighboring cells. The cell density independence of this signal suggests that the signal is not transport mediated, and the fact that the signal strength increases with flow rate suggests the possibility that the signal is mechanically mediated, reminiscent of shear-induced directional migration of endothelial cells, discussed below.

At high cell density, signals secreted by neighboring cells interfere with the autocrine chemokine field, and the magnitude of autocrine transcellular gradients are affected by neighboring cells. A similar effect can occur at high Pe: ligands from upstream cells are washed downstream and can interact with the autocrine chemokine fields of downstream cells, reducing the magnitude of autocrine transcellular gradients. We believe this explains the peak at 0.3μm/s for streamline and directional migration scores of cells with functional CCR7. At low seeding densities and flow rates, interstitial flow induces a transcellular autocrine gradient resulting in a higher percentage of bound CCR7 receptors downstream and consequently, a downstream chemotactic signal. However, at higher seeding densities and flow rates, these autocrine gradients become noisy, and the strength of the chemotactic signal is reduced, and the competing signal dominates causing fewer cells to migrate along the streamline and increasing upstream migration bias.

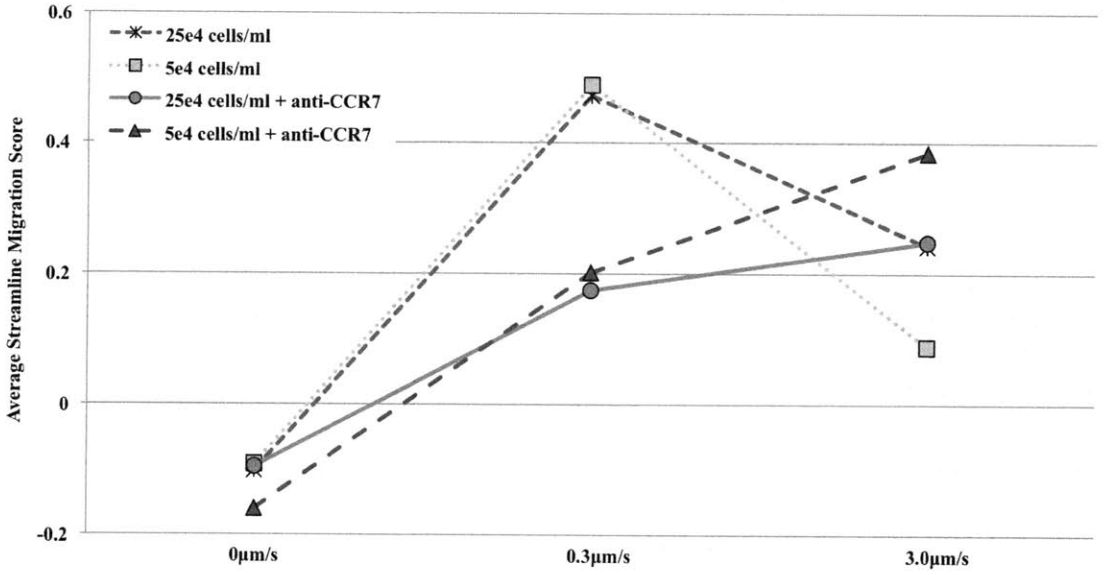

Figure 42: Average streamline migration score for each experimental condition. Error bars are omitted for clarity. Note peak at 0.3µm/s for cells with functional CCR7 receptors.

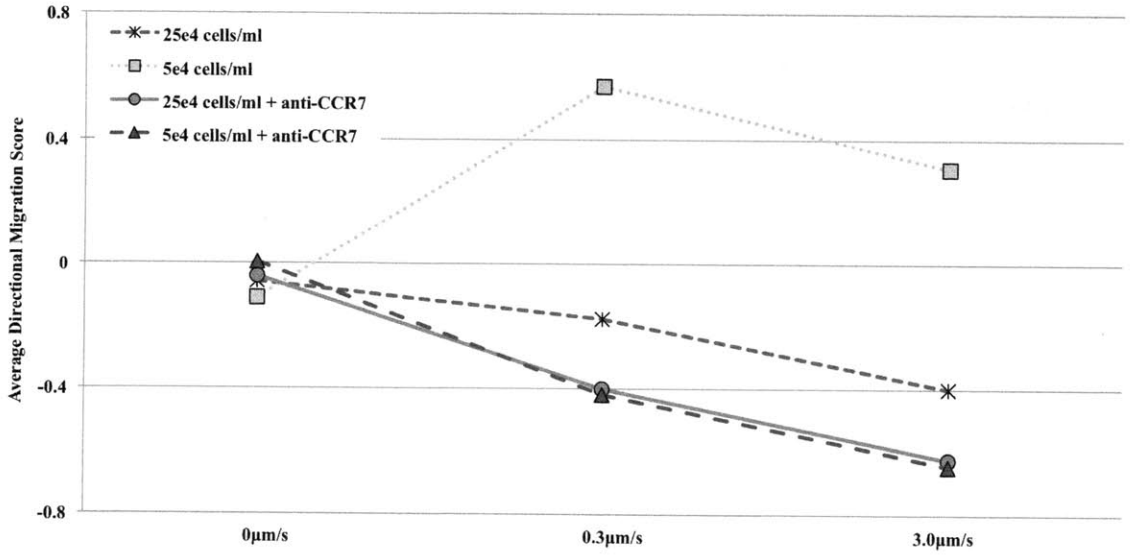

Figure 43: Average directional migration score for each experimental condition. Note that seeding density does not affect migration directional bias when CCR7 is blocked.

5.8. Shear stress and mechanotransduction

Shear stress has long been postulated to play a role in endothelial cell (EC) migration (68). Much recent work *in vitro* and *in vivo* has focused on identifying molecular and mechanical mechanisms by which ECs can detect and respond to flow-induced shear stress (66-72). It has been shown that flow can induce directional EC migration and that this directional migration is important in physiologic processes such as wound healing (66). These studies demonstrated that the cell response is mechanically mediated; cells can detect flow through shear-induced strain on the cell membrane and intracellular cytoskeleton. Recent work has demonstrated that fluid flow can strain the ECM and this strain can be translated to the cytoskeleton by mechanical junctions known as focal adhesions (73, 75). *In vitro* experiments have demonstrated that these various mechanical signals can induce cytoskeletal restructuring and even guide cell migration. This process by which cells detect a mechanical signal and modulate biological processes in response to the signal is known as mechanotransduction (73, 76).

Mechanotransduction has long been known to be crucial in regulating EC function, and recent work has demonstrated its importance in cancer. However, little work has been done to investigate mechanotransduction in response to fluid flow on cancer cells. Furthermore, because much work on shear stress and mechanotransduction has been to understand its role in the context of ECs and blood vessels, most *in vitro* studies have been constrained to 2D flow assays to mimic the lumen of vasculature.

We suspect that the mechanics of flow-induced migration are significantly different in 3D. For example, in 3D, the pressure drop across the length of the cell can lead to significant forces at the upstream side of the cell (Figure 44, 51). It has also been shown, that direct application of force

to the surface of a cell increases the stiffness of the cytoskeleton and can lead to clustering of focal adhesion (FA) complexes, and clustering of FA complexes is associated with directional migration of cells (74). Although modeling and experimentation are needed to understand the mechanical stimuli from interstitial flow to cells seeded in 3D matrix, we suspect mechanotransduction serves a major role in modulating the cell response to interstitial flow.

We hypothesize that mechanotransduction could provide the competing stimulus to CCR7-dependent autologous chemotaxis and drive cells upstream. A mechanical stimulus would be a function of flow rate and, unlike a transport mediated stimulus, independent of cell density. Thus we hypothesize CCR7-dependent autologous chemotaxis and a mechanical stimulus leading to mechanotransduction govern cell migration in the presence of interstitial flow.

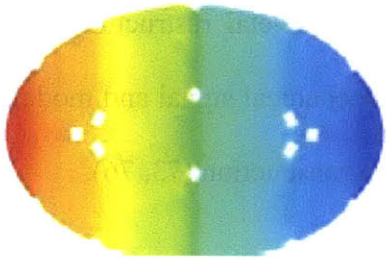

Figure 44: Model of pressure gradient on a cell surface induced by interstitial flow. Flow is from left to right, red indicates maximum force, blue indicates minimum force. High force on the surface of the cell can induce FA formation and directional migration (adapted from 51).

5.9. Other possible competing pathways

Although we suspect that mechanotransduction leads to upstream migration, we realize that interstitial flow could induce a variety of other stimuli to cells. It is possible that shear stress induces non-uniform receptor distribution and resulting receptor binding causes a chemotactic response even in the presence of near uniform concentration gradients. However, we do not think shear-induced receptor distribution is likely to be a significant stimulus in our system as it should

be cell-density dependent. More experiments, including receptor-binding assays, are required to test this hypothesis. Interacting paracrine and autocrine cheomkine concentration fields can result in bulk concentration gradients for certain cell concentrations, flow rates, and matrix binding interactions. As each downstream cell subsequently adds more ligand to the bulk fluid, the ligand concentration can be much greater downstream than upstream. If cells are secreting chemorepellant, such a bulk concentration gradient would induce an upstream chemotactic response. However, few chemorepellants, particularly breast cancer secreted chemorepellants, are known. Secretome assays would be required to test this hypothesis.

It is also possible that matrix metalloproteases (MMPs) are being washed downstream. MMPs break down matrix to allow cell migration. A bulk concentration gradient of MMP could lead to a mechanical stiffness gradient in the gel. Breast cancer cells are known to exhibit durotaxis (56-58), and consequently, the mechanical stiffness gradient in the collagen gel could lead to upstream migration. However, reflectance confocal imaging does not seem to indicate any gradients in matrix integrity. Further modeling and experimentation, including static MMP gradient assays, would be required to examine this hypothesis.

6. Conclusion

Our microfluidic device design has allowed rigorous examination of interstitial flow as a migrational stimulus. We developed a system that allowed repeatable application of an interstitial flow field to cells seeded in 3D matrix. We showed that interstitial flow has profound effects on the bias in direction of migrating breast cancer cells. We provide supporting evidence to the autologous chemotaxis model, and extend the model to include effects on downstream directional bias of migrating cells. We demonstrated that a competing mechanism drives cell migration upstream and our data on migration as a function of flow rate and cell density suggests this stimulus is mechanically mediated, inducing migration through mechanotransduction. With further modeling and experimentation we hope to provide insight into this mechanism and its interplay with CCR7-dependent autologous chemotaxis. In summary, we provide evidence that interstitial flow is a powerful morphoregulator and stimulus for tumor cell migration.

Appendix I – Migration bias expressed as fractions of migrating cells

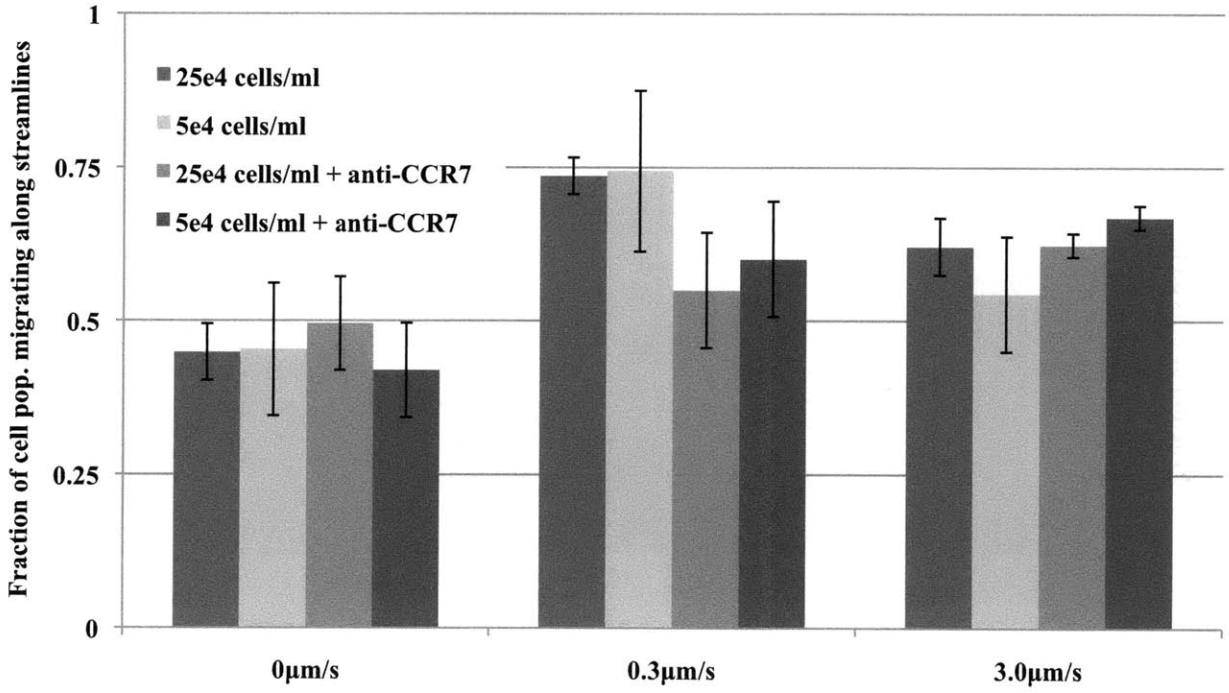

Figure 45: Fraction of cell population migrating along streamline for each set of experimental conditions.

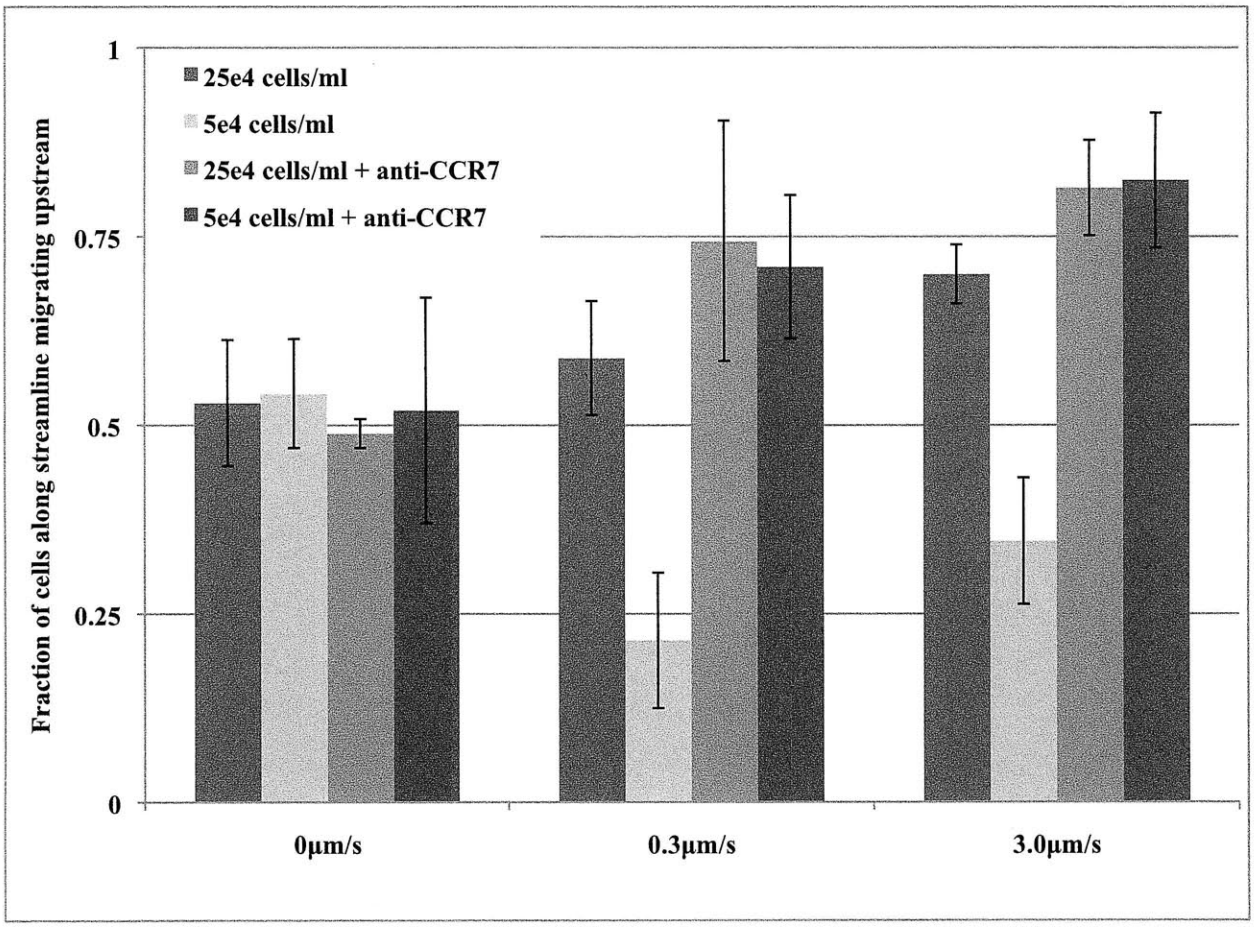

Figure 46: Of cells migrating along streamline, the fraction of cells migrating upstream.

Appendix II – Total streamline and directional migration scores

Because there are a variety of test conditions, elucidating trends based on the pair-wise comparisons presented above can become tedious and confusing. Below are a series of tables and figures meant to summarize the directional migration data. Table 1 includes the mean values for the average streamline migration metric and average directional migration metric for each test condition. Table 2 provides the p-value for a one-way ANOVA performed between the two test conditions labeled 'vs.' Every possible permutation of test condition is considered, and the p-values are meant to facilitate comparing test conditions. Figure 47 graphically illustrates the streamline migration metric for each test condition. Statistical significance is indicated between relevant groups. Finally, Figure 48 graphically illustrates the directional migration metric for each test condition. These tables and figures will be used in conjunction with the pair-wise comparisons from the previous results sections to identify interesting and significant trends in the data.

Table 1: Summary of streamline and directional scores for cell populations (mean±SEM)

Antibody	Cell/ml	Flow Rate	Average Streamline	Average Directional
None	25e4	0μm/s	-0.102±0.05	-0.06±0.1
None	25e4	0.3μm/s	0.472±0.03	-0.177±0.09
None	25e4	3.0μm/s	0.242±0.023	-0.401±0.05
None	5e4	0μm/s	-0.092±0.06	-0.111±0.11
None	5e4	0.3μm/s	0.489±0.07	0.57±0.10
None	5e4	3.0μm/s	0.10±0.10	0.307±0.096
anti-CCR7	25e4	0μm/s	-0.096±0.05	-0.041±0.077
anti-CCR7	25e4	0.3μm/s	0.174±0.040	-0.401±0.098
anti-CCR7	25e4	3.0μm/s	0.248±0.044	-0.628±0.072
anti-CCR7	5e4	0μm/s	-0.160±0.068	0.005±0.11
anti-CCR7	5e4	0.3μm/s	0.202±0.018	-0.420±0.100
anti-CCR7	5e4	3.0μm/s	0.384±0.050	-0.650±0.102

Table 2: Summary of comparisons between experimental conditions. P-values given from student's t-test.

Antibody	Cells/ml	Flow Rate	Streamline	Directional
None	25e4	vs.	0.0052	0.0855
None	5e4	vs.	0.0366	0.1525
None	vs.	0.3μm/s	0.84	0.0053
None	vs.	3.0μm/s	0.2372	0.0016
vs.	25e4	0.3μm/s	0.0311	0.2013
vs.	25e4	3.0μm/s	0.911	0.0465
vs.	5e4	0.3μm/s	0.01	0.0025
vs	5e4	3.0μm/s	0.0687	0.0018
CCR7	25e4	vs.	0.2757	0.5164
CCR7	5e4	vs.	0.0268	0.2753
CCR7	vs.	0.3μm/s	0.4095	0.8966
CCR7	vs.	3.0μm/s	0.1126	0.8797

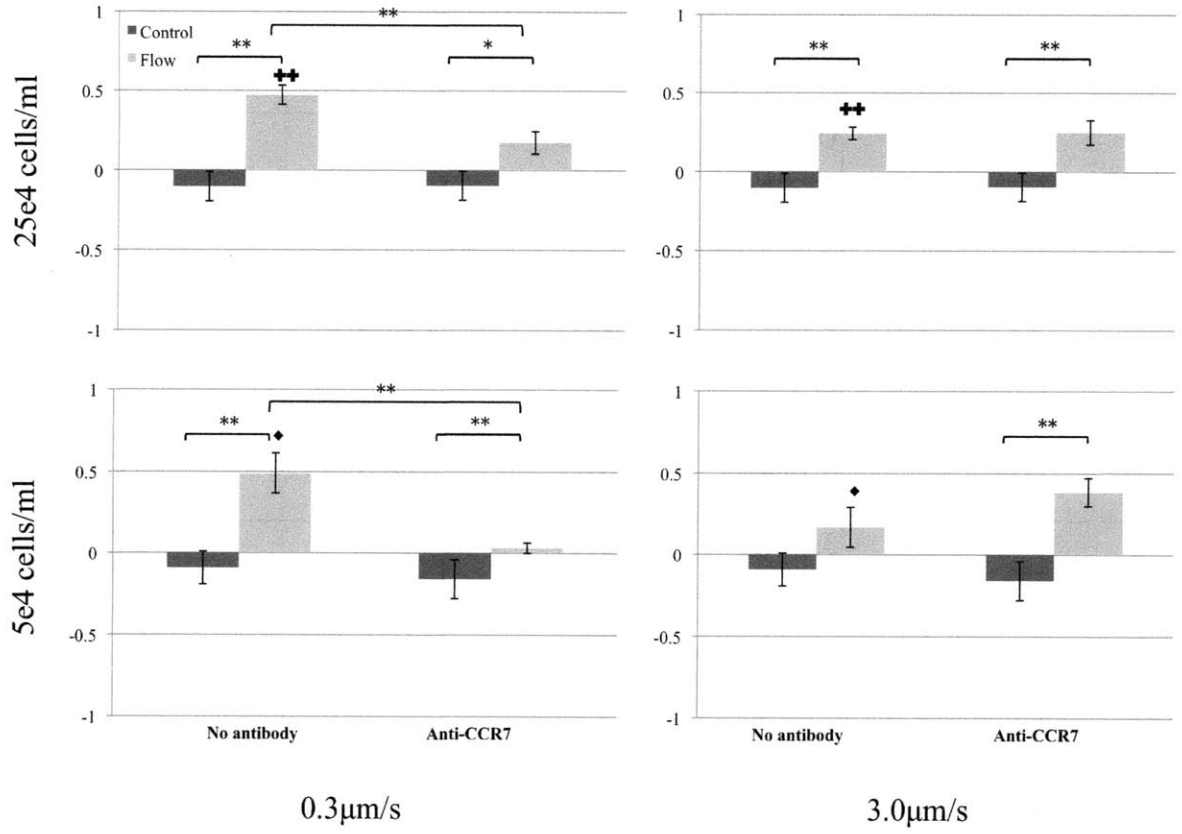

Figure 47: Summary of streamline migration scores for cells at each experimental condition. (◆,✚ indicate significance for similarly labeled data sets)

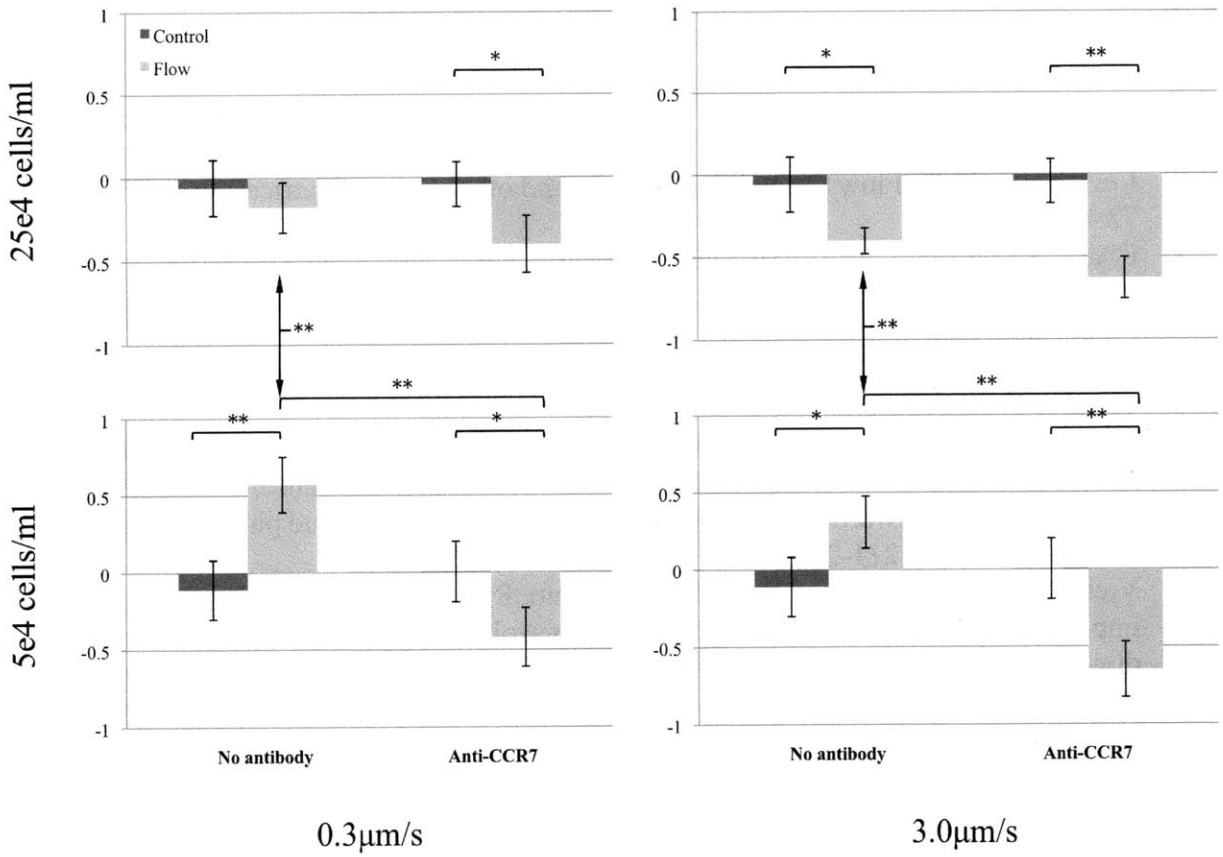

Figure 48: Summary of directional migration scores for cells at each experimental condition.

References:

1. Swartz, MA and Fleury, ME. 2007. Interstitial flow and its effects in soft tissues. Annu. Rev. Biomed. Eng. 9:229-56.
2. Levick, JR. 1987. Flow through interstitium and other fibrous matrices. Q. J. Exp. Phys. 72:409-37.
3. Chary, SR and Jain, RK. 1989. Direct measurement of interstitial convection and diffusion of albumin in normal and neoplastic tissues by fluorescence photobleaching. Proc. Natl. Acad. Sci. 86:5385-89.
4. Heldin, C, Rubin, K, Pietras, K, and Östman, A. 2004. High interstitial fluid pressure – an obstacle in cancer therapy. Nat. Rev. Cancer. 4:806-13.
5. Shields et al. 2007. Autologous chemotaxis as a mechanism of tumor cell homing to lymphatics via interstitial flow and autocrine CCR7 signaling. Cancer Cell. 11:526-38
6. Griffith, LG, and Swartz, MA. 2006. Capturing complex 3D tissue physiology *in vitro*. Nat. Rev. MCB. 7:211-24.
7. Vickerman, V, Blundo, J, Chung, S, and Kamm, RD. 2008. Design, fabrication and implementation of a novel multi-parameter control microfluidic platform for three-dimensional cell culture and real-time imaging. Lab on a Chip. 8:1468-77.
8. Fleury, ME, Boardman, KC, and Swartz, MA. 2006. Autologous morphogen gradients by subtle interstitial flow and matrix interactions. Biophysical Journal. 91:113-21.
9. Dafni, H, Israely, T, Bhujwalla, Z, Benjamin, L, and Neeman, M. 2002. Overexpression of vascular endothelial growth factor 165 drives peritumor interstitial convection and induces lymphatic drain: magnetic resonance imaging, confocal microscopy, and histological tracking of triple-labeled albumin. Cancer Research. 62:6731-6739.
10. Wang, S and Tarbell, JM. 2000. Effect of fluid flow on smooth muscle cells in a 3-dimensional collagen gel model. Arterioscler. Thromb. Vasc. Biol. 20:2220-2225.
11. Ng, CP and Swartz, MA. 2003. Fibroblast alignment under interstitial fluid flow using a novel 3-D tissue culture model. Am. J. Phiol. Heart Circ. Physiol. 284:H1771-H1777.
12. Brinkman, HC. 1947. A calculation of the viscous force exerted by a flowing fluid on a dense swarm of particles. Appl. Sci. Res. A1:27-34.
13. Bakal, C, Aach, J, Church, G and Perrimon, N. 2007. Local signaling networks that regulate cell morphology defined by quantitative morphological signatures. Science. 316:1753-1576.
14. Cordelires, F. 2004. Manual Tracking plugin for ImageJ.
15. Muller, A, et al. 2001. Involvement of chemokine receptors in breast cancer metastasis. Nature. 410: 50-56.
16. Roskelley, C.D., Desprez, P.Y. and Bissell, M.J. 1994. Extracellular matrix-dependent tissue-specific gene expression in mammay epithelial cells requires both physical and biochemical signal transduction. Proc. Natl. Acad. Sci. 91: 12378-12382.
17. Bissell, M.J., Rizki, A. and Mian, I.S. 2003. Tissue architecture: the ultimate regulator of breast epithelial function. Curr. Opin. Cell Biol. 15:753-762.
18. Wozniak, M.A., Desai, R., Solski, P.A., Der, C.J. and Keely, P.J. 2003. ROCK-generated contractility regulates breast epithelial cell differentiation in response to the physical properties of a three-dimensional collagen matrix. J. Cell Biol. 163: 583-595.
19. Peyton, S.R. and Putnam, A.J. 2005. Extracellular matrix rigidity governs smooth muscle cell motility in a biphasic fashion. J. Cell Physiol. 204: 198-209.

20. Paszek, M.J. *et al.* 2005. Tensional homeostasis and the malignant phenotype. Cancer Cell. 8: 241-254.
21. Boardman, K.C. and Swartz, M.A. 2003. Interstitial flow as a guide for lymphangiogenesis. Circ. Res. 92:801-808.
22. Boucher, Y., Laurence, B.T. and Jain, R.K. 1990. Interstitial pressure gradients in tissue-isolated and subcutaneous tumors: implications for therapy. Cancer Research. 50:4478-4484.
23. Chambers, A.F., Groom, A.C. and MacDonald, I.C. 2002. Dissemination and growth of cancer cells in metastatic sites. Nature Reviews. 2:563-573.
24. Weigelt, B., Peterse, J.L. and van't Veer, L.J. 2005. Breast cancer metastasis: markers and models. Nature Reviews. 5:591-603.
25. Christofori, G. 2006. New signals from the invasive front. Nature. 44:444-451.
26. Fidler, I.J. 2003. The pathogenesis of cancer metastasis: the 'seed and soil' hypothesis revisited. Nat. Rev. Cancer. 3:1-7.
27. Friedl, P. and Brocker, E.B. 2000. The biology of cell locomotion within three-dimensional extracellular matrix. Cell Mol. Life Sci. 57:41-64
28. Chen, Y. Stamatoyannopoulos, G., and Song, C.Z. 2003. Down-regulation of CXCR4 by inducible small interfering RNA inhibits breast cancer cell invasion *in vitro*. Cancer Research. 63:4801-4804.
29. Liu, Y. Ji, R. Li, J., Giang, G., Xiulan, Z., Sun, T., Wang, J., Li, J., Du, Q. and Sun, B. 2010. Correlation effect of EGFR and CXCR4 and CCR7 chemokine receptors in predicting breast cancer metastasis and prognosis. J. Exp. Clin. Cancer Res. 29:16-25.
30. Muller, A. et al. 2001. Involvement of chemokine receptors in breast cancer metastasis. Nature. 410:50-57.
31. Chang, S., Chang, C.A., Lee, D., Lee, P., Yeh, Y., Yeh, C., Cheng, C., Chien, S. and Chiu, J. 2008. Tumor cell cycle arrest induced by shear stress: roles of integrins and Smad. Proc. Nat. Acad. Sci. 105:3927-2932.
32. Cabioglu, N., Yazici, M.S., Arun, B., Broglio, K.R., Hortobagyi, G.N., Price, J.E. and Sahin, A. 2005. CCR7 and CXCR4 as novel biomarkers predicting axillary lymph node metastasis in T_1 breast cancer. Human Canc. Bio. 16:5686-5694.
33. Walker, G.M., Sai, J., Richmond, A., Stremler, M., Chung, C.Y. and Wikswo, J.P. 2005. Effects of flow and diffusion on chemotaxis studies in a microfabricated gradient generator. Lab on a Chip. 5:611-618.
34. Saadi, W., Wang, S., Lin, F. and Jeon, N.L.2006. A parallel-gradient microfluidic chamber for quantitative analysis of breast cancer chemotaxis. Biomed Microdevices. 8:109-118.
35. Keenan, T.M. and Folch, A. 2007. Biomolecular gradients in cell culture systems. Lab on a Chip. 8:34-57.
36. Keenan, T.M. 2006. Microfluidic "jets" for generating steady-state gradients of soluble molecules on open surfaces. App. Phys. Letters. 89:114103-1-114103-3.
37. Jeon, N.L., Dertinger, S.K.W., Chiu, D.T., Choi, I.S., Stroock, A.D. and Whitesides, G.M. 2000. Generation of solution and surface gradients using microfluidic systems. Langmuir. 16:8311-8316.
38. Hegerfeldt, Y., Tusch, M., Brocker, E. and Friedl, P. 2002. Collective cell movement in primary melanoma explants: Plasticity of cell-cell interaction, β1-Integrin function and migration strategies. Cancer Res. 62:2125-2130.

39. Wolf, K., Wu, Y.I., Liu, Y.L., Geiger, J., Tam, E., Overall, C., Stack, M.S. and Friedl, P. 2007. Multi-step pericellular proteolysis controls the transition from individual to collective cancer cell invasion. Nature Cell Biol. 9:893-913.
40. Friedl, P., Hegerfeldt, Y. and Tusch, M. 2004. Collective cell migration in morphogenesis and cancer. Int. J. Dev. Biol. 48:441-449.
41. Friedl, P. et al. 1995. Migration of coordinated cell clusters in mesenchymal and epithelial cancer explants *in vitro*. Cancer Research. 55:4557-4560.
42. Waters, C.M., Oberg, K.C., Carpenter, G. and Overholser, K.A. 1990. Rate constants for binding, dissociation, and internalization of EGF: effect of receptor occupancy and ligand concentration. Biochemistry. 29:3563-3569.
43. Bailly, M., Wyckoff, J., Bouzahzah, B., Hammerman, R., Sylvestre, V., Cammer, M., Pestell, R. and Segall, J.E. 2000. Epidermal growth factor receptor distribution during chemotactic responses. Mol. Biol. of the Cell. 11:3873-3883.
44. Jain, R.K. 1987. Transport of molecules in the tumor interstitium: a review. Cancer Research. 47:3039-3051.
45. Hofmann, M., Guschel, M., Bernd, A., Bereiter-Hahn, J., Kaufmann, R., Tandi, C., Wiig, H. and Kippenberger, S. 2006. Lowering of tumor interstitial fluid pressure reduces tumor cell proliferation in a xenograft tumor model. Neoplasia. 8:89-95.
46. Helm, C., Fleury, M., Zisch, A.H., Buschetti, F. and Swartz, M.A. 2005. Synergy between interstitial flow and VEGF directs capillary morphogenesis *in vitro* through a gradient amplification mechanism. Proc. Nat. Acad. Sci. 44:15779-15784.
47. Boucher, Y. and Jain, R.K. 1992. Microvascular pressure is the principal driving force for interstitial hypertension in solid tumors: implications for vascular collapse. Cancer Research. 52:5110-5114.
48. Helm, C.E., Zisch, A. and Swartz, M.A. 2006. Engineered blood and lymphatic capillaries in 3-D VEGF-fibrin-collagen matrices with interstitial flow. Biotech. and Bioeng. 96:167-176.
49. He, Y., Karpanen, T. and Alitalo, K. 2004. Role of lymphangiogenic factors in tumor metastasis. Biochimica et Biophysica Acta. 1654:3-12.
50. Carmeliet, P. 2003. Angiogenesis in health and disease. Nat. Med. 9:653-660.
51. Pedersen, J.A., Licther, S. and Swartz, M.A. 2010. Cells in 3D matrices under interstitial flow: effects of extracellular matrix alignment on shear stress and drag forces. 43:900-905.
52. Mierke, C.T. et al. 2008. Breakdown of the endothelial barrier function in tumor cell transmigration. Biophysical Journal. 94:2832-2846.
53. Leunig, M., Yuan, F., Menger, M.D., Boucher, Y., Goetz, A.E., Messmer, K. and Jain, R.K. 1992. Angiogenesis, microvasculature architecture, microhemodynamics, and interstitial fluid pressure during early growth of human adenocarcinoma LS174T in SCID mice. Cancer Research. 52:6553-6560.
54. Even-Ram, S. and Yamada, K.M. 2005. Cell migration in 3D matrix. Curr. Op. Cell Biol. 17:524-532.
55. Chan, C.E. et al. 2008. Traction dynamics of filopodia on compliant substrates. Science. 322:1687-1692.
56. Fischbach, C., Kong, H.J., Hsiong, S.X., Evangelista, M.B., Yuen, W. and Mooney, D.J. 2009. Cancer cell angiogenic capability is regulated by 3D culture and integrin engagement. Proc. Nat. Acad. Sci. 106:399-404.

57. Lazopoulos, K.A. and Stamenovic, D. 2008. Durotaxis as an elastic stability phenomenon. Journal of Biomech. 41:1289-1294.
58. Zaman, M.H. et al. 2006. Migration of tumor cells in 3D matrices is governed by matrix stiffness along with cell-matrix adhesion and proteolysis. Proc. Nat. Acad. Sci. 29:10889-10894.
59. Krohn, A., Song, Y., Muehlber, F., Droll, L., Beckmann, C. and Alt, E. 2009. CXCR4 receptor positive spheroid forming cells are responsible for tumor invasion *in vitro*. Cancer Letters. 280:65-71.
60. Price, J.T., Tiganis, T., Agarwal, A., Djakiew, D. and Thompson, E.W. 1999. Epidermal growth factor promotes MDA-MB-231 breast cancer cell migration through a phosphatidylinositol 3'-kinase and phospholipase C-dependent mechanism. Cancer Research. 59:5475-5478.
61. Wang, S., Saadi, W., Lin, F., Nguyen, C.M. and Jeon, N.L. 2004. Differential effects of EGF gradient profiles on MDA-MB-231 breast cancer cell chemotaxis. Exp. Cell Res. 300:180-189.
62. Tranquillo, R.T., Lauffenburger, D.A. and Zigmond, S.H. 1988. A stochastic model for leukocyte random motility and chemotaxis based on receptor binding fluctuations. J. Cell Biol. 106:303-309.
63. Xia, Y. and Whitesides, G.M. 1998. Soft lithography. Ann. Rev. Mat. Sci. 28:153-184.
64. Park, T.H. and Shuler, M.L. 2003 Integration of cell culture and microfabrication technology. Biotechnol. Prog. 19:243-253.
65. Meyvantsson, I. and Beebe, D.J. 2008. Cell culture models in microfluidic systems. Ann. Rev. of Analytical Chem. 1:423-449.
66. Li, S., Huang, N.F. and Hsu, S. 2005. Mechanotransduction in endothelial cell migration. J. of Cellular Biochem. 96:1110-1126.
67. Boardman, K.C. and Swartz, M.A. 2003. Interstitial flow as a guide for lymphangiogensis. Circ. Res. 92:801-808.
68. Branemark, P.I. 1965. Capillary form and function. The microcirculation of granulation tissue. Bibl. Anat. 7:9-28.
69. Moldovan, N.I, Goldschmidt-Clermont, P.J., Parker-Thornburg, J., Shapiro, S.D. and Kolattukudy, P.E. 2000. Contribution of monocytes/macrophages to compensatory neovascularization: The drilling of metalloelastase-positive tunnels in ischemic myocardium. Circ. Res. 87:378-384.
70. Galbraith, C.G., Skalak, R. and Chien, S. 1998. Shear stress induces spatial reorganization of the endothelial cell cytoskeleton. Cell. Motil. Cytoskeleton. 40:317-330.
71. Helmke, B.P., Goldman, R.D., Davies, P.F. 2000. Rapid displacement of vimentin intermediate filaments in living endothelial cells exposed to flow. Circ. Res. 86:745-752.
72. Wang, N., Butler, J.P. and Ingber, D.E. 1993. Mechanotransduction across the cell surface and through the cytoskeleton. Science. 260:1124-1127.
73. Li, S., Kim, M., Hu, Y.L., Jalali, S., Schlaepfer, D.D., Hunter, T., Chien, S. and Shyy, J.Y. 1997. Fluid shear stress activation of focal adhesion kinase. Linking to mitogen-activated protein kinases. J. Biol. Chem. 272:30455-30462.
74. Tsuruta, D. and Jones, J.C. 2003. The vintemin cytoskeleton regulates focal contact size and adhesion of endothelial cells subjected to shear stress. J. Cell Sci. 16:4977-4985.

75. Critchley, D.R. 2000. Focal adhesions – The cytoskeletal connection. Curr. Opin. Cell Biol. 12:133-139.
76. Li, S., Butler, P., Wang, Y., Hu, Y., Han, D.C., Usami, S., Guan, J.L. and Chien, S. 2002. The role of the dynamics of focal adhesion kinase in the mechanotaxis of endothelial cells. Proc. Natl. Acad. Sci. 99:3546-3551.